

pubs.acs.org/JPCB Perspective

## **Photophysical Engineering of Fluorescent Proteins:** Accomplishments and Challenges of Physical Chemistry Strategies

Srijit Mukherjee and Ralph Jimenez\*



Cite This: J. Phys. Chem. B 2022, 126, 735-750



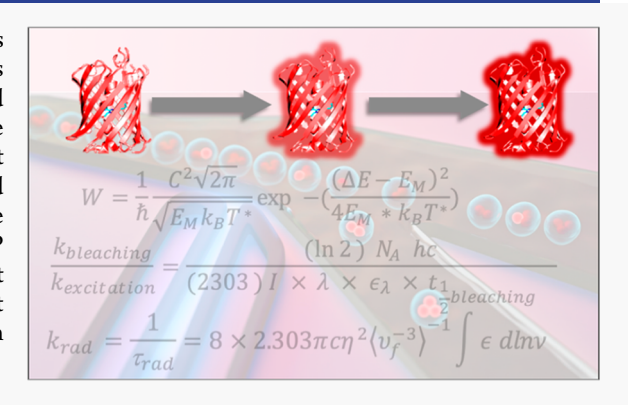
ACCESS I



Metrics & More

Article Recommendations

ABSTRACT: Fluorescent proteins (FPs) have become ubiquitous tools for biological research and concomitantly they are intriguing molecules that are amenable to study with a wide range of experimental and theoretical tools. This perspective explores the connection between the engineering of improved FPs and basic ideas from physical chemistry that explain their properties and drive the molecular design of brighter and more photostable variants. We highlight some of the progress and the many knowledge gaps in understanding the relationship between FP brightness and photostability. We also explore some of the pertinent remaining questions and suggest ways in which physical chemists might further examine the physical basis of brightness and photostability in these systems.



## 1. INTRODUCTION

Since the first isolation of naturally occurring fluorescent proteins (FPs) from marine organisms several decades ago, subsequent developments in protein engineering have produced a large family of fluorophores spanning the entire visible wavelength spectrum.<sup>1,2</sup> Applications of FPs in bioimaging and sensing include multicolor microscopy, Förster resonance energy transfer (FRET)-based tools,<sup>4</sup> fluorescence lifetime imaging microscopy (FLIM),5 voltage sensing,<sup>6</sup> biosensing,<sup>7</sup> catalytic activity monitoring,<sup>8</sup> aggregation studies,<sup>9</sup> and nonbiophysical applications such as biophosphors for LED lighting.<sup>10</sup> Additionally, the engineering of FPs exhibiting reversible and photoactivated fluorescence and photoswitching between fluorescence bands has enabled imaging with spatial resolution beyond Abbe's diffraction limit. Despite and because of this widespread use, development of new FPs continues. For example, with the increasing interest in deep-tissue imaging of live animals, significant efforts have focused on the discovery and development of brighter red FPs (RFPs), as longer excitation and emission wavelengths generally provide lower scattering and increased penetration-depth.

FP engineering is inextricably tied to consideration of protein structure. Fortunately, hundreds of X-ray crystallographic structures of FPs at atomic resolution are available (e.g., Figure 1). In the canonical green fluorescent protein superfamily, the chromophore—which is comparable in size to synthetic small-molecule fluorophores (~1 nm)—is contained inside a  $\beta$ -barrel with an internal  $\alpha$ -helix. <sup>12</sup> Several chromophore variants can be autocatalytically formed from

the reaction of O<sub>2</sub> with a tripeptide in this helix. One common structure typically comprises p-hydroxyphenyl and imidazolinone moieties connected by a methylidyne bridge (Figure 1). The electronic conjugation across this hydrolyzed tripeptide results in a chromophore with a  $\pi \to \pi^*$  electronic transition excitable at visible wavelengths. The chromophore participates in numerous interactions with amino acids and the solvent. These short-range interactions (e.g., hydrogen bonding) or long-range effects (e.g., electric fields) tune the energetics and control the electronic structure of the chromophore. Accordingly, amino acid substitutions, sometimes surprisingly distant from the chromophore, perturb its electronic structure, influence the energetics of its electronic transition, and cause changes in its conformation and the nuclear degrees of freedom coupled to it. Additionally, the overall protein structure governs the movement of diffusing species such as water or O2, which can also lead to alterations in chromophore properties. In general, it is difficult to separate the impacts of numerous variables that nonadditively contribute to the photophysics. All these factors should be taken into consideration for explaining and tuning properties such as brightness and photostability. 13-16

Received: June 26, 2021 January 4, 2022 Revised: Published: January 25, 2022





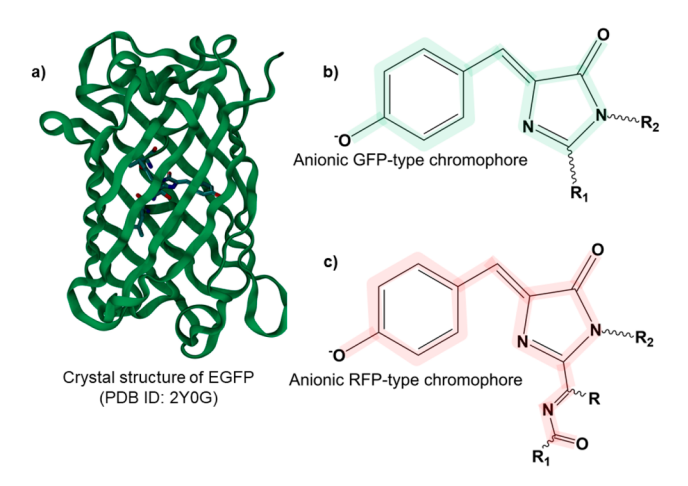


**Figure 1.** (a) Crystal structure for enhanced GFP (EGFP; PDB ID: 2Y0G) showing the  $\beta$ -barrel encompassing the internal helix and the chromophore, for which oxygen atoms are indicated in red, nitrogen in blue and carbon in gray. (b) Ground state structure of the anionic GFP-type p-hydroxyphenyl—imidazolinone chromophore (c) Ground state structure of the anionic RFP p-hydroxyphenyl—imidazolinone chromophore showing the extension of the electronic conjugation through an acylimine moiety. Green and red highlighting indicate the bonds participating in electronic conjugation (resonance) across the chromophore. Structures were generated using VMD and ChemDraw software suites. <sup>26,27</sup>

In addition to being useful for imaging, FPs provide an incredible molecular framework for investigating diverse photophysical, spectroscopic and dynamical phenomena such as solvation dynamics, light harvesting, photoinduced excited state intramolecular proton and electron transfer, photo-

transformations such as photoisomerization, and other radiationless transitions.  $^{17-20}$  One can examine them with biochemical or physical methods by combining spectroscopic measurement tools including steady-state and time-resolved optical and vibrational spectroscopy, with structural approaches such as nuclear magnetic resonance (NMR) and both static and time-resolved X-ray crystallography. Here, we will discuss the development of FPs, focusing on topics that may be of interest to physical chemists. Though we will focus on the GFP superfamily, the topics discussed below apply to FPs of other lineages, such as those containing tetrapyrrole chromophores. <sup>21–23</sup> We further center discussion on brightness and photostability, which are arguably the most rudimentary fluorophore properties. As described below, it has been a difficult task to optimize them in tandem. 16 Studies of the principles behind brightness and photostability have been pursued in our lab for over a decade, and they provide a platform for discussing far more general concepts. For discussion of more complex functionalities, such as photoactivation and photoswitching, we refer readers to other reviews. <sup>24,25</sup> In describing some of the biggest successes, notable failures, and remaining challenges, we also consider the role of physical principles in guiding design strategies.

## 2. BRIGHTNESS

**2.1.** Approaches for Improving Brightness. Fluorescence brightness is a molecular property defined as the product of the molar extinction coefficient at maximum absorption  $(\epsilon_{\text{max}})$  and the fluorescence quantum yield  $(\Phi)$ . However, when FPs are imaged in cells, the observed cellular brightness is a consequence of additional factors such as protein folding, kinetics of chromophore maturation, translational efficiency, expression level (i.e., concentration), environmental sensitivity

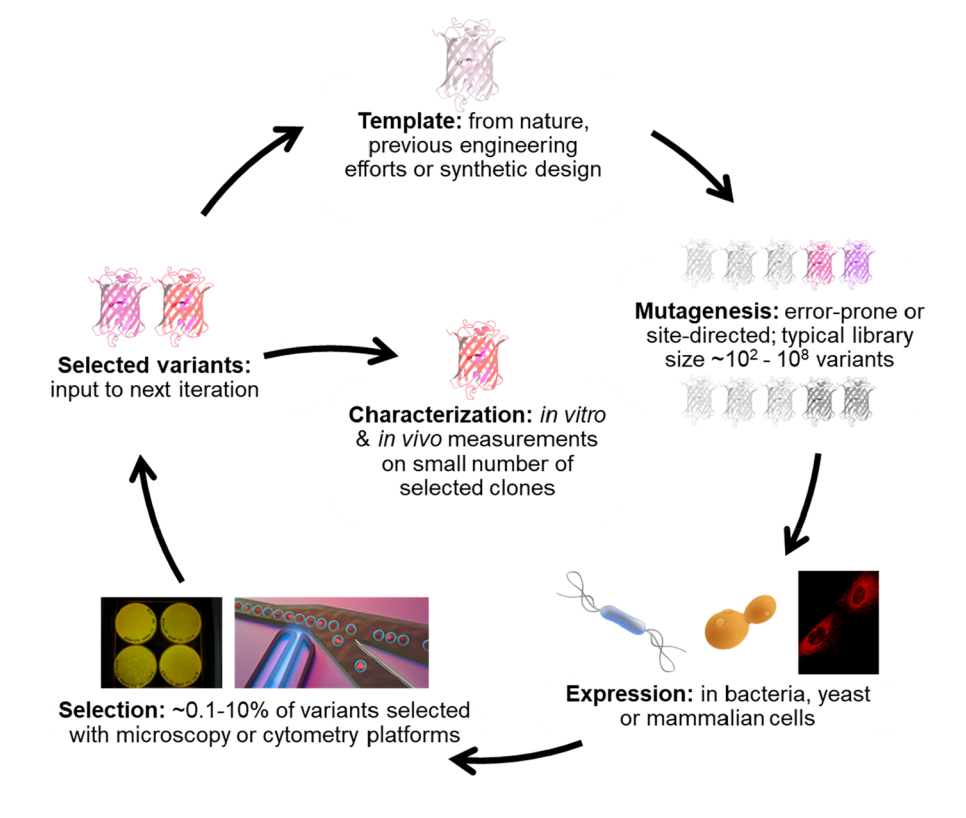


Figure 2. Schematic representation of the process for engineering genetically encodable fluorescent biomarkers employed in our group.

to pH, nature of the fusion-protein construct and chemical environment of the cellular compartment.<sup>28</sup> The typical development pipeline for improving brightness or other FP properties involves generating "libraries" (which may range in size from dozens to > 10<sup>7</sup> variants) using error-prone PCR or site-directed mutagenesis based on structural, spectroscopic and bioinformatics guidance (Figure 2). These libraries are then typically expressed in a host, such as bacteria, yeast, or mammalian cells that allows for screening and selection of clones with desired characteristics—such as higher brightness. For example, fluorescence activated cell sorting (FACS) and fluorescence imaging are popular tools for selecting on cellular brightness. The mutation and selection cycles are repeated to achieve "directed evolution" in terms of the selection pressure.<sup>29</sup> After several rounds, a small number of selected clones are expressed, and the purified FPs are individually characterized to determine values of molecular properties such as the fluorescence quantum yield and peak molar extinction coefficient. This approach has yielded substantially improved FPs such as EGFP<sup>30</sup> (1.7-fold brighter than progenitor avGFP) and the mRubys<sup>31</sup> (mRuby3; 1.7-fold brighter than the naturally occurring progenitor eqFP511), of which the best have peak molar extinction coefficients and fluorescence quantum yields comparable to those of small-molecule dyes. For example, mNeonGreen<sup>32</sup> has fluorescence quantum yield  $\sim$  80% and a  $\epsilon_{\rm max}$  at  $\sim$ 116 000 M $^{-1}$ cm $^{-1}$  (brightness of  $\sim$ 93) with a peak absorption wavelength comparable to the recently developed, xanthene-based Janelia Fluor (JF) dye JF-503, which has a fluorescence quantum yield  $\sim$  87% and an  $\epsilon_{\rm max}$   $\sim$ 95 000  $M^{-1}$ cm<sup>-1</sup> (brightness ~ 83).<sup>33</sup>

Despite the historical success of this approach, alternative strategies for obtaining brighter FPs have been explored, particularly in recent years as the pace of improvements has slowed. For example, the choice of template has garnered increased attention. In most cases, the template is either a naturally occurring FP or a commonly used FP that has undergone previous rounds of development. The notable exception is the brightest RFP as of early 2021, mScarlet, which was developed from a synthetic gene template.<sup>34</sup> Given this achievement, one might be tempted to think natural templates have reached their limits. However, Lambert et al. (2020) reported the discovery of AausFP1, a naturally occurring GFP from the jellyfish Aequorea victoria, from which the original GFP was obtained.35 This FP has the highest ever reported value of fluorescence quantum yield (97%) and a peak molar extinction coefficient of  $\sim 170\,000$ M<sup>-1</sup> cm<sup>-1</sup>. Although the dimeric structure and the very small Stokes shift of AausFP1 may limit its use for imaging, these defects could be addressed, and this discovery suggests that nature will continue to be a source for brighter fluorophores.

Many FPs have been optimized for specific biochemical applications (for example, cellular localization or pH sensitivity) and engineering photophysically improved variants mandates keeping close attention to their *in vivo* attributes. For instance, Campbell and co-workers proposed that GFP-based fluorophores with the glycine-tyrosine-glycine (G-Y-G) tripeptide chromophore might have attained a local maximum of molecular brightness. Consequently, they focused on improving properties that can increase cellular brightness, such as solubility, translation efficiency, protein folding, and chromophore maturation. With this approach, they developed mGreenLantern, which is 6-fold brighter in mammalian cells than EGFP. This improvement in cellular brightness came

without an appreciable change in the molecular brightness from its precursor FP - Clover.<sup>36</sup> This study demonstrates that increasing cellular brightness by generating a fast-maturing FP with high copy number can be beneficial in some applications, such as imaging of neurons. However, we found that imaging of small subcellular structures, such as the Golgi apparatus, sometimes benefits more from controlled expression of FPs with high molecular brightness.<sup>37</sup> This suggests that improvements of both molecular and cellular brightness should be pursued in tandem.

The selection step (Figure 2) is of particular interest to physical chemists because spectroscopic measurements, such as fluorescence lifetime  $(\tau)$ , can be incorporated on platforms that allow high-throughput screening of cells, such as microfluidic or microscopy-based systems. 29,34,37,38 Relationships between sequence, structure and any spectroscopically accessible property can be investigated by this approach on 10<sup>7</sup> or more variants per day. Fluorescence lifetime-based screening in particular has proven useful because lifetime is independent of concentration, and it is correlated with higher molecular brightness (with caveats, see below). Lifetime-based selection on a microscopy platform led to the development of mScarlet from the dim synthetic template mRed7.<sup>34</sup> Our lab has pioneered the integration of microfluidic flow cytometry with photobleaching, photoswitching, and fluorescence lifetime selection.<sup>39–43</sup> For example, we employed a cell sorter based on fluorescence lifetime to variants of FusionRed with 3-fold higher molecular brightness.<sup>37</sup>

Few efforts have directly aimed to alter the absorption properties by tuning the oscillator strength of electronic transitions in FPs, but initial results in this direction are promising. 44,45 In a recent study, Myšková and co-workers determined transition dipole moments of absorption (xTDM) and emission (mTDM) of several well-studied, bright FPs. 46 Their approach combined cryogenic X-ray crystallography with room-temperature polarized optical transmission and fluorescence measurements to determine the orientation of these dipole moments. By characterizing the propensity of FPs to crystallize into specific space groups with certain molecular orientations, the authors were able to interpret the optical measurements with two well-defined assumptions. They assumed the TDM of the chromophore was in plane of the two aromatic rings and furthermore that there is a cosinesquared relationship of the TDM with the polarized absorption or fluorescence intensity. Information from such studies can inform development of FPs for applications that are sensitive to the directions of the transition dipoles, such as FRET. Another study based on considering the transition dipole moments was reported by Molina et al. (2020) who developed a high-throughput, fluorescence microscope-based screening device (GIZMO) for screening bacterial cells by two-photon excited fluorescence.<sup>47</sup> The two-photon absorption crosssection can be used to examine the radiative rate and electric fields around the chromophore (the effects of internal electric fields on FP photophysics is discussed below). GIZMO is capable of screening  $10^4$  bacterial cells in  $\sim$ 7 h, demonstrating great potential for this type of selection in the directed evolution of FPs.

Unconventional selection strategies that do not directly measure brightness have also been explored to develop brighter FPs. For example, many FPs exhibit two-state (on/off) "blinking" of their fluorescence intensities at the single molecule level. These transitions occur when the chromophore

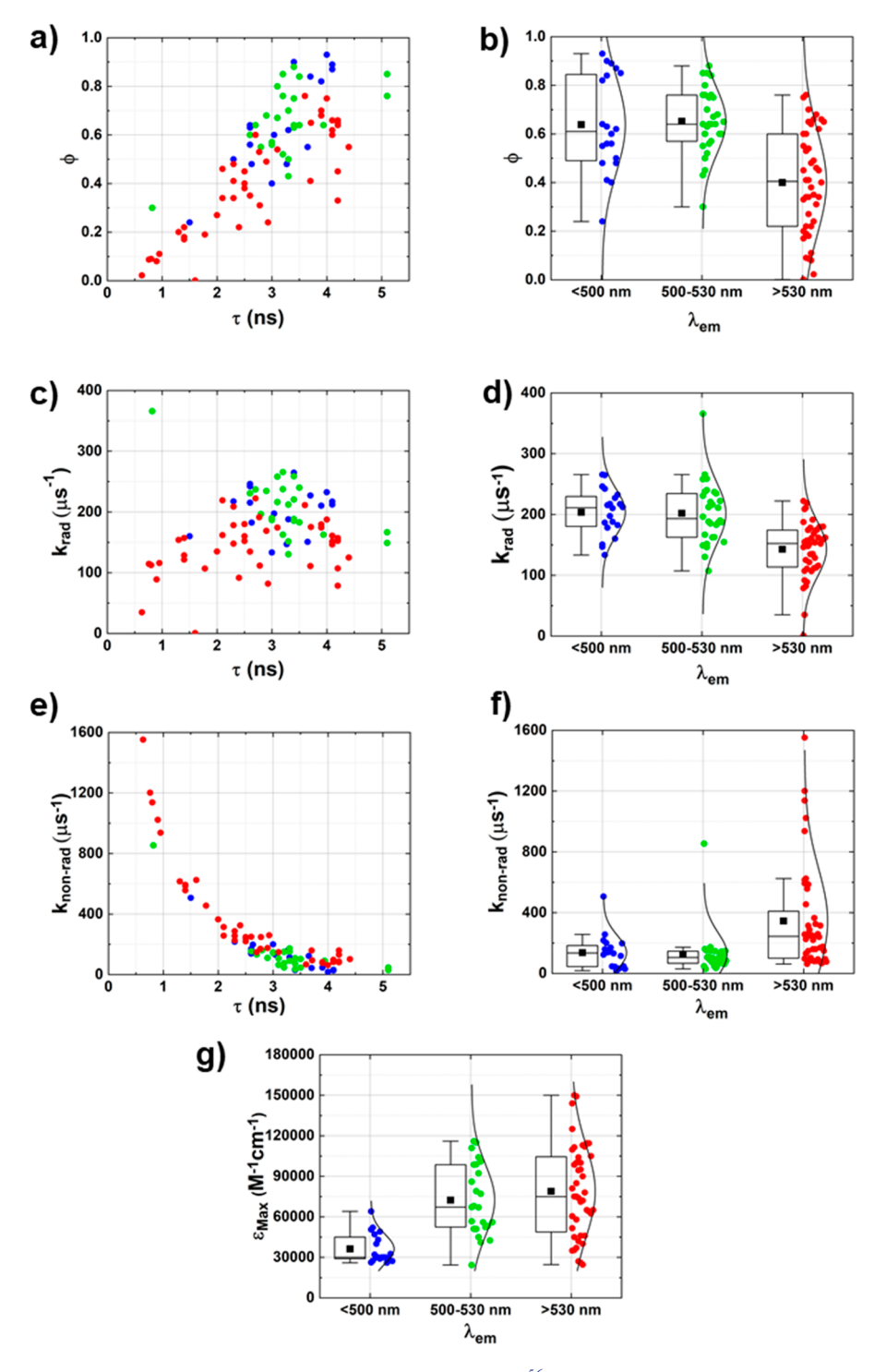


Figure 3. Photophysical data from 89 published FPs were obtained from FPBase. So along with values for FusionRed-Q, -MQ, and -MV variants from ref 37. Points in blue indicate FPs with peak emission wavelength  $\lambda$  < 500 nm, green with peak emission wavelength in the range 500 nm <  $\lambda$  < 530 nm, and red with peak emission wavelength  $\lambda$  > 530 nm. The boxplots indicate the distributions of values: the mean of the distribution is indicated by black solid squares, the box indicates the 25th and 75th percentiles, and the whiskers indicate the 5th and 95th percentiles of the distribution. The solid line in the box indicates the median value of the distribution. (a, b) Trends for the fluorescence quantum yield ( $\Phi$ ): Increases in fluorescence lifetime ( $\tau$ ) generally correlate with a higher fluorescence quantum yield. (c, d) Trends for radiative rate constant ( $k_{\rm rad}$ ): There is a  $\sim$  5-fold variation in the radiative rate constant—where a higher wavelength emission can potentially lead to lower radiative rate values. The GFP BruSLEE stands out as an exception ( $k_{\rm rad}$  > 350 us<sup>-1</sup>). (e, f) Trends for the nonradiative rate constant ( $k_{\rm nonrad}$ ): The nonradiative rates decrease up to  $\sim$  50-fold with increasing lifetime. The observed values indicate the means and the standard deviations of  $k_{\rm nonrad}$  Blue  $\sim$  137  $\pm$  112  $\mu$ s<sup>-1</sup>;  $k_{\rm nonrad}$  Green  $\sim$  130  $\pm$  158  $\mu$ s<sup>-1</sup>;  $k_{\rm nonrad}$  Red  $\sim$  346  $\pm$  345  $\mu$ s<sup>-1</sup>. (g) Trends for the peak extinction coefficient: Red emitting FPs tend to exhibit larger peak extinction coefficients than green and blue counterparts due to chromophore extension by the acylimine moiety.

has access to nonfluorescent excited electronic states with microsecond to millisecond lifetimes. This "dark state

conversion" (also sometimes referred to as "reversible photobleaching") leads to rapid blinking, and the depopulation

of the ground state can result in an apparent reduction in brightness. This connection between blinking, dark-state conversion, and brightness has been exploited. In particular, FLINC (fluorescence fluctuation increase by contact)—an imaging technique with 3-fold higher resolution than the diffraction limit, is based on the observation that the blinking frequency of TagRFP-T varies ~ 25% as a function of the length of a linker peptide altering its spatial proximity to the nonfluorescent Dronpa FP. 48 Charged residues on the  $\beta$ -barrel participate in electrostatic interactions that control the dark state conversion rates. Consequently, libraries were developed by targeting positions with externally facing side chains (acidic D159, D196 and basic R157, R198) and selections on reduced rate of dark-state conversion through FLINC were successful for developing SuperTag-RFP, which is 2-fold brighter than TagRFP-T.49

The properties of new variants must be characterized carefully to avoid potential misapplications, e.g., in imaging modalities for which the photophysical properties are unsuitable. For example, population transfer to dark states can be a bottleneck for continuous excitation, especially at high irradiances. Dark states typically are related to chromophore conformational changes or intersystem crossing to the triplet state, and lead to trapping on time scales several orders of magnitude longer than an excitation-emission cycle. 50,51 For detailed discussions of this topic, we refer readers to reviews on dark state conversion and related phototransformations such as photoswitching. 16,52 On a practical note, dark state conversion, which is distinct from saturation of the optical transition in a 2level system, can lead to inaccuracies in measurements of fluorescence quantum yield, as shown by Ruhlandt and coworkers for photoswitching FPs.<sup>53</sup> Partially in response to this complication, Prangsma and co-workers developed methods to accurately determine the fluorescence quantum yield by tuning the local photon density of states near a metal surface. Looking beyond the influences on brightness, investigations of dark-state conversion and engineering of fluorescence blinking are valuable for probe development in super-resolution microscopy. It remains challenging to measure the rates of dark-state conversion, ground-state recovery, and photobleaching which, depending on the FP, may vary by many orders of magnitude (and may overlap in time scales) over the wide range of irradiances relevant to imaging, even for variants with closely related sequences. 54,55

**2.2.** The Photophysical Basis of Increased Brightness. 2.2.a. General Principles. The improved molecular brightness of many newer FPs is attributable to increases in fluorescence quantum yield  $(\Phi)$  and fluorescence lifetime  $(\tau)$ . (Figure 3a) Consider the relationship between the fluorescence quantum yield and the radiative  $(k_{\rm rad})$  and nonradiative  $(k_{\rm nonrad})$  rate constants:

$$\Phi = k_{rad} \times \tau \tag{1}$$

$$\Phi = \frac{k_{rad}}{(k_{rad} + k_{nonrad})} \tag{2}$$

In principle, a particular value of fluorescence lifetime can arise from different combinations of values of  $k_{\rm rad}$  and  $k_{\rm nonrad}$ . We extracted lifetime and quantum yield data from the online repository FPBase <sup>56</sup> to estimate radiative and nonradiative rates. We assumed the reported lifetime values from FPBase can be used to estimate the radiative and nonradiative rates, despite the use of multiple measurement techniques, with FPs

in different environments (in vitro vs. in vivo), and the use of average values to represent what is typically a multiexponential decay. The analysis reveals only a 5-fold variation in the values of the radiative rate constant but a 50-fold variation in the values of the nonradiative rate constant (Figure 3c vs Figure 3e). A similar observation for a small set of RFPs was made by Drobizhev et al. 57 Furthermore, a correlation of higher fluorescence quantum yields with longer fluorescence lifetime is clear, though the relationship is not perfectly linear. While a higher fluorescence quantum yield most often seems to be due to a lower nonradiative rate constant, increasing the radiative rate constant also increases fluorescence quantum yield, as seen for BrUSLEE (evident as out-lying points in Figure 3a and Figure 3c).<sup>58</sup> This EGFP variant exhibits a short fluorescence lifetime of 0.8 ns but a relatively high fluorescence quantum yield (30%), with a 1.6-fold increase in the radiative rate constant. Mamontova et al., achieved this by reducing the fluorescence lifetime of EGFP while maintaining its brightness. They isolated a triple mutant EGFP T65G-Y145M-F165Y, with spectral properties similar to EGFP, but with a 20% lower brightness and a 70% shorter fluorescence lifetime (cf. 2.6 ns for EGFP). Although this result shows that radiative rate engineering is possible, molecular strategies to guide the design have not been reported. In this context, we briefly consider well-known models for radiative and nonradiative transitions.

The Radiative Rate Constant ( $k_{rad}$ ). The experimentally observable parameters underlying the magnitude of radiative rate can be seen in the Strickler–Berg relationship

$$k_{rad} = \frac{1}{\tau_{rad}} = 8 \times 2.303\pi c \eta^2 \langle v_f^{-3} \rangle^{-1} \int \epsilon \, \mathrm{d}(\ln \nu)$$
(3)

which shows that the radiative rate is linearly proportional to the squared value of the refractive index of the medium containing the chromophore  $(\eta)$ , the strength of the optical transition to the excited electronic state ( $\int \epsilon d(\ln \nu)$ ; where  $\epsilon$  is the extinction coefficient integrated over the absorption band), the inverse of the mean inverse-cubed emission frequency  $(\langle v_f^{-3} \rangle^{-1})$ , and c denotes the speed of light.<sup>59</sup> For chromophores with relatively narrow fluorescence spectra, the cube of the peak fluorescence frequency is  $\nu_{peak}^{-3} \sim \langle v_f^{-3} \rangle^{-1.57}$  The Strickler–Berg equation shows that strong absorbers have higher radiative rates than weakly absorbing chromophores. As a secondary effect, there is a linear dependence of radiative rate on the cube of the fluorescence frequency. 60 A long wavelength emitter will radiate slower than a shorter wavelength emitter with the same integrated absorption cross-section embedded in a medium of the same refractive index. Although this dependence does not represent a direct relationship to the Stokes shift, it does indicate that blue shifting the peak emission can increase the radiative rate. Equation 3 is qualitatively in agreement with Figure 3d. The extension of the electronic conjugation through the acylimine moiety is likely to be the largest factor in making red FPs stronger absorbers. However, Figure 3g shows that many green FPs absorb as strongly as red FPs. The increased extinction coefficient of the red chromophore can be partially offset by the lower frequency emission to decrease the radiative rates.

Lin et al. found good agreement with the Strickler–Berg equation for a set of GFP variants involving residues directly interacting with or forming the chromophore. These FPs showed a nearly constant radiative rate and an inverse relationship of the peak molar extinction coefficient with the width of the absorption band. The first observation is

consistent with the trend seen in parts c and e of Figure 3, where the variation in radiative rates is much smaller compared to the variation in nonradiative rates. Accordingly, they suggest that large changes in the fluorescence quantum yields of FPs are unlikely to be the result of variations in  $k_{\rm rad}$ . However, the example of BrUSLEE shows that tuning the radiative rate by protein engineering is possible. EGFP and BrUSLEE have nearly identical absorption and emission spectra and peak wavelengths, and the increased molar extinction coefficient ( $\epsilon_{\rm max}$ ) and radiative rate constant of BrUSLEE follow what is expected from the Strickler–Berg relationship: a  $\sim 1.5$ -fold higher value of  $\epsilon_{\rm max}$  results in a  $\sim 1.6$ -fold increase of the radiative rate.

A final point that should be made about the Strickler-Berg equation is that it might be inaccurate to assume the refractive indices of FPs hardly vary. We used eq 3 and the spectral data from FPbase to calculate values of  $\eta$  for blue (Cerulean), green (EGFP), and red (mScarlet) FPs, all three of which show nearly monoexponential fluorescence lifetime decays in aqueous environments.<sup>56</sup> The refractive indices show the expected trend of increasing value with decreasing wavelength, but the increase is considerably larger than expected ( $\eta_{
m mScarlet}$   $\sim$ 1.21;  $\eta_{\rm EGFP} \sim 1.25$ ;  $\eta_{\rm Cerulean} \sim 1.49$ ). The refractive index of water only varies by 2% over this wavelength range. 62 The sensitivity of FP fluorescence lifetime to refractive index has been explored as a sensing technique in cellular environments. 63 These observations may provide a route for design of FPs with increased radiative rate by exploring a connection with the polarizability of the amino acids comprising the  $\beta$ -

The Nonradiative Rate Constant ( $k_{nonrad}$ ). In the absence of photochemistry, excited-state nonradiative population loss follows two major routes, internal conversion (IC), and intersystem crossing (ISC). The factors influencing the probability of the transition  $W_{12}$  can be described by Fermi's Golden Rule (eq 4).

$$W_{12} = \frac{2\pi \left| M_{12} \right|^2}{\hbar} \rho_2 \tag{4}$$

For IC between the initial (1) and the final (2) vibronic states of the two electronic manifolds,  $M_{12}$  is the matrix-element for the electronic interaction that couples them, and  $\rho_2$  is the density of vibrational states of the final configuration. This expression also applies to the rate of ISC to a triplet state. In highly fluorescent FP chromophores the ISC rate is much smaller than IC due to a change in the spin multiplicity. Investigations of ISC and triplet states in FPs merit further attention as such states can play a pivotal role in oxidative photochemistry and photobleaching.

While eq 4 accounts for the physics of the nonradiative transition rate, it does not provide useful insight for FP engineering. Reports on new fluorophores mention a dependence of the nonradiative transition rate on the  $S_1$ – $S_0$  transition energy (i.e., the "energy-gap law") which results from further theoretical development. The classic theory of Englman and Jortner provides a framework for understanding nonradiative transition rates in terms of experimental observables such as the electronic energy gap ( $\Delta E$ ), the Stokes shift (from vibrational reorganization) and vibrational frequencies. Their theory makes assumptions very similar to those of Marcus theory of electron transfer, and population transfer between weakly coupled initial and final states occurs by means

of environmental fluctuations. This approach considers the high and low temperature limits of strong and weak coupling between the chromophore vibrations and electronic transitions. The low temperature limit,  $\hbar\langle\omega\rangle\gtrsim k_BT$  is defined in terms of the mean vibrational frequency  $\langle\omega\rangle=N^{-1}\sum_j\omega_j$ , where N is the number of modes and  $\omega_j$  is the frequency of each mode. In the low temperature - strong coupling regime, the coupling strength  $G\sim\frac{E_M}{\hbar\langle\omega\rangle}>1$ . Here,  $E_{\rm M}\sim$  Stokes shift/2 in the absence of excited state processes such as excited state proton transfer (ESPT). In the low-temperature/strong coupling limit, the expression for the nonradiative rate resembles that derived by Marcus for the electron transfer rate:

$$W = \frac{1}{\hbar} \frac{C^2 \sqrt{2\pi}}{\sqrt{E_M k_B T^*}} \exp -\left(\frac{(\Delta E - E_M)^2}{4E_M^* k_B T^*}\right)$$
 (5)

 $T^*$  is the effective vibrational temperature  $T^* \sim \hbar \langle \omega \rangle / k_B$ ,  $C (\sim 10^2 - 10^4 \text{ cm}^{-1})$  represents the Herzberg–Teller coupling of the vibronic transition, and the other variables were previously defined. With experimental Stokes shifts from below 300 cm<sup>-1</sup> to above 3000 cm<sup>-1</sup> and energy gaps from below 15000 cm<sup>-1</sup> to 22500 cm<sup>-1</sup>, FPs can theoretically fall into either weak or strong coupling cases or in between them. For the weak coupling limit (G < 1) suited to most FPs, the observed Stokes shift is severalfold smaller than electronic transition energy ( $\Delta E$ ). In this case, one arrives at the following expression for the nonradiative rate:

$$W = \frac{1}{\hbar} \frac{C^2 \sqrt{2\pi}}{\sqrt{\hbar \omega_M \Delta E}} \exp -\left(\frac{\gamma \Delta E}{\hbar \omega_M}\right)$$
(6)

Here,  $\omega_M$  is the frequency of the normal mode vibration with the maximum frequency in the chromophore, the parameter  $\gamma \sim \log\left(\frac{\Delta E}{d\epsilon_m}\right) - 1$ ; where d is the degeneracy and  $e_m$  is a

measure of the reorganization energy of this vibrational mode in the excited state. While more applicable to FPs, the weak-coupling form is less intuitive in its relation to experimental observables. Further theoretical work is necessary to address the both and possible intermediate regimes of this formalism in the context of FP engineering. Both strong and weak-coupling regimes indicate that the nonradiative transfer probability (W) is dependent on the Stokes shift (from vibrational reorganization), vibrational frequencies that couple to the electronic transition and the transition energy gap. To illustrate the effects of these parameters on the nonradiative rate, we plot the trends expected from the weak coupling expression in Figure 4, which shows that decreasing energy gap and increased reorganization energy lead to an increased nonradiative decay rate (W).

The Englman—Jortner approach can qualitatively explain the difference in average nonradiative rate for GFPs relative to RFPs. The lower energy emission of the latter is due to their larger chromophores. RFPs contain an acylimine moiety over which the electronic conjugation is extended compared to GFPs (Figure 1, parts b and c). The larger number of vibrational degrees of freedom and smaller electronic energy gap of RFPs could possibly lead to a higher density of states. One can thus predict RFPs to have lower fluorescence quantum yields than GFPs, in-part due to the expected higher values of the nonradiative rate constant. However, an outstanding exception to this trend is mScarlet, which has a

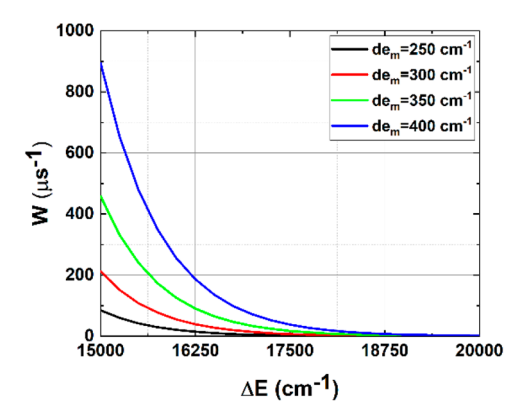


**Figure 4.** Expected trends from the weak-coupling low temperature limit of Englman–Jortner theory (eq 6): The superexponential increase of the nonradiative rate (W) for smaller energy gaps ( $\Delta E$ ) and larger reorganization energies (de<sub>m</sub>). The values  $\omega_M \sim 3000~{\rm cm}^{-1}$  and  $C^2 \sim 10^7~{\rm cm}^{-2}$  were fixed, as discussed in ref 68

smaller nonradiative rate constant than many bright blue-shifted counterparts such as EGFP ( $k_{\rm nonrad~mScarlet} \sim 77~\mu {\rm s}^{-1}$  vs  $k_{\rm nonrad~EGFP} \sim 113~\mu {\rm s}^{-1}$ ), <sup>56</sup> despite a significantly lower  $\Delta E$  (by  $\sim 3000~{\rm cm}^{-1}$ ) and near identical values of  $E_{\rm M}$  ( $\sim 375~{\rm cm}^{-1}$ ). This RFP was designed with a focus on conformationally restricting the chromophore, which could have resulted in a lower density of accessible vibrational states in the ground electronic state. <sup>34</sup> The causes of this exceptional behavior merit further investigation. Further theoretical and experimental studies are warranted to examine the extent to which energy-gap effects are the main contributor to nonradiative relaxation especially in red and far-red emitting chromophores. <sup>57</sup>

Spectral Features. In the descriptions of Strickler-Berg and Englman-Jortner models for the rates of radiative and nonradiative transitions, we pointed out where correlations with steady-state spectral properties are to be expected. For example, small Stokes shifts and blue-shifted emission peaks are correlated with high radiative rates and low nonradiative rates. The Stokes shift reflects the reorganization energy for solvation of the excited electronic state (half of the Stokes shift =  $E_{\rm M}$ , as in eqs 5 and 6) but this is correct only in the absence of excited state photochemistry such as excited state proton transfer (ESPT) which occurs in the "large Stokes shift (LSS)" FPs. In addition to absorption and emission peak values, photophysical properties are correlated with absorption lineshapes and line widths. Chromophore spectral lineshapes are sensitive to the underlying femtosecond to nanosecond time scale protein and solvent dynamics and protein conformational heterogeneity. Ultrafast spectroscopy experiments such as time-resolved fluorescence Stokes shift measurements and photon echo techniques resolve the time scales of nuclear motions. 70,71 An understanding of the interplay between protein structure and dynamics would provide useful insight for FP engineering efforts.<sup>72</sup> To date, most ultrafast spectroscopy of FPs has focused on investigating excited-state photoreactions such as chromophore isomerization, ESPT, and hydrogen-bond dynamics (see below). We now turn to a consideration of structural features and mechanisms for excited state depopulation, such as hydrogen bonding and electrostatic effects.1

2.2.b. Discussion of Specific Cases. Structural Arguments. Often, the rationale for mutations to improve brightness is centered on trying to make the chromophore more "planar"

and the FP more "rigid." It is expected from molecular orbital arguments that a planar or flatter chromophore would result in stronger  $\pi \to \pi^*$  electronic transitions and thus a larger value of extinction coefficient due to improved electronic delocalization through the methine bridge.<sup>73</sup> The second rationale is difficult to examine critically due to the complexity of quantifying "rigidity." Furthermore, the existence of a conical intersection in the excited-state potential energy surface of FPs, linked to the twisting of the methine bonds between the two rings complicates the straightforward picture of planarity and rigidity.<sup>74</sup> Although they are not certain to capture the average chromophore conformation or excited state distortions, X-ray crystal structures show a correlation between chromophore planarity and brightness. 16 The structures of mCherry and mStrawberry revealed that the decreased fluorescence quantum yield of these FPs are correlated with nonplanarity of these chromophores compared to the parent DsRed and sibling mOrange.<sup>75</sup> The X-ray crystal structure of mScarlet (PDB ID:5LK4) shows a dihedral angle of  $\sim 1.9^{\circ}$  between the methine bridge and phenol ring (or the P-bond rotation), which is significantly smaller than the  $\sim 13.1^{\circ}$  for the dimmer RFP mCherry (PDB ID:2H5Q).<sup>34</sup> The flatter chromophore has a  $\sim$ 1.5-fold higher  $\epsilon_{\rm max}$   $\sim$ 3-fold higher fluorescence quantum yield, ~2.5-fold higher radiative rate constant, and ~7-fold lower nonradiative rate constant. Along these lines, mutagenesis to introduce residues that improve the packing around the chromophore have often been used to generate brighter variants. This strategy was employed in the development of mTurquoise2, where a fluorescence quantum yield of 93% (the highest of all engineered FPs) was achieved by introducing an I146F substitution in mTurquoise (fluorescence quantum yield  $\sim$  84%). This residue was identified as a target for mutagenesis by a combination of fluorescence lifetime screening, X-ray crystallography, and classical MD simulations, which suggested that a bulkier, nonpolar residue might restrict the conformational freedom of the chromophore, resulting in a higher fluorescence quantum yield.

Inspiration for molecular design has been provided by spectroscopic and theoretical studies of specific interactions and excited-state processes in relation to hydrogen bonding and proton transfer - particularly in GFP model chromophores. 77-79 While a majority of these studies have been based on a combination of vibronic spectroscopy, computational methods, X-ray crystal structure analysis and bioinformatics, NMR and electron paramagnetic resonance spectroscopy have also proven useful (and perhaps underutilized) for providing further insight into FP structure and conformational dynamics. 84-86 For example, high-resolution 2D <sup>1</sup>H-<sup>15</sup>N solution-based NMR backbone relaxation study revealed a light-induced conformational change in the photoswitchable protein rsFolder.87 The use of kinetic crystallography for revealing the structural transitions associated with long-lived dark states has also been fruitful.<sup>88</sup> This promising approach combines real-time crystallization of FP molecules with optical measurements such as Raman spectroscopy. The work of Bourgeois and co-workers has provided insights into the mechanisms behind phototransformations in photoswitchable FPs like mEos4B.<sup>89</sup> A structural perspective can be helpful for identifying specific interactions that might govern brightness. 16-19

Influence of Local Hydrogen-Bonding Networks. Though hydrogen bonding has a variety of impacts on the photophysics of various types of FP chromophores, we will limit our

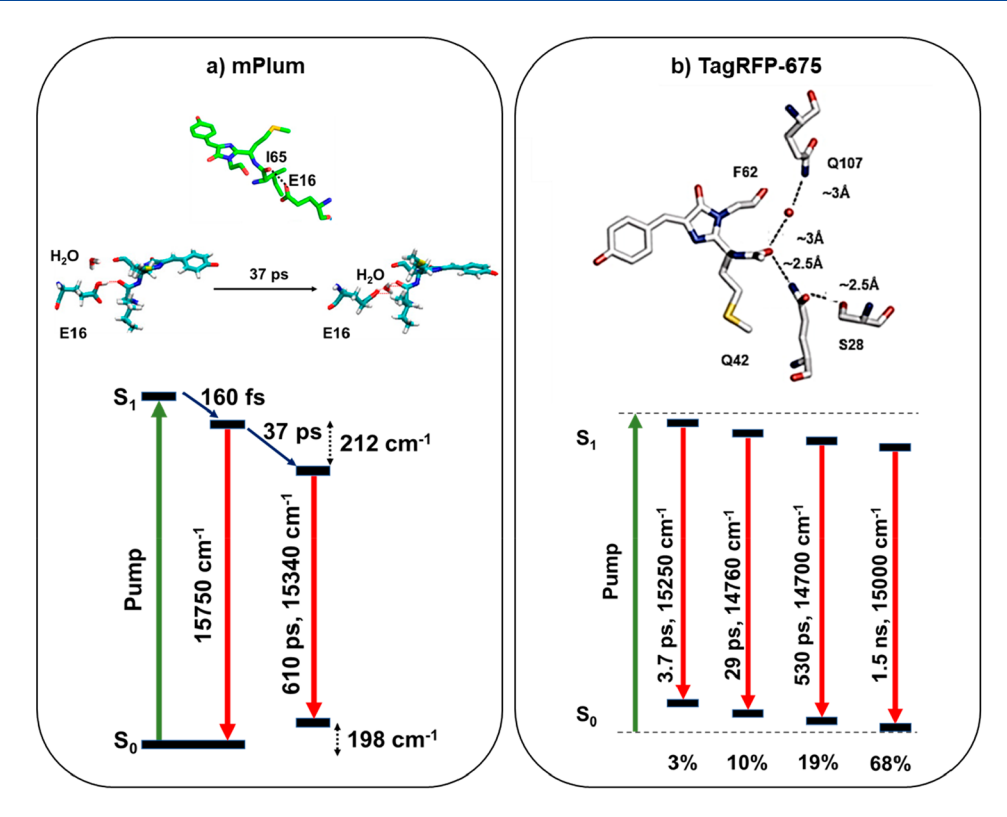


Figure 5. Excited-state spectral and structural dynamics in RFPs studied using ultrafast spectroscopy. (a) mPlum: Two-state interconversion of direct and water-mediated hydrogen-bonding states.  $^{78,90,92}$  (b) TagRFP-675: The side chains of residues F62-Q42-Q107-S28-R41 constitute a hydrogen-bonding network leading to four spectral forms (with populations given as percentages) and widely varying excited-state  $\tau$ .  $^{15}$ 

considerations to RFPs, and in particular the role of hydrogen bonding with regard to the acylimine moiety. In RFPs, the introduction of a single hydrogen-bonding interaction with the acylimine moiety was proposed for red-shifting the emission. However, the major outcome of this new motif is the introduction of picosecond time scale conformational changes which influence the brightness and the Stokes shift of emission. These processes have been investigated both with experiments and QM/MM simulations. <sup>15,78,90-92</sup> In mPlum, which has a large 1540 cm<sup>-1</sup> (60 nm) Stokes shift, Boxer and co-workers observed a picosecond time scale red shift of the emission spectrum, which they explained as a dynamic Stokes shift associated with reorganization of the E16 hydrogen bond.<sup>93</sup> We used time-resolved fluorescence experiments to reveal the two-state interconversion between the direct and watermediated hydrogen-bonding interactions of the acylimine with the E16 residue (Figure 5a).<sup>78</sup> QM/MM simulations confirmed the connection between the structural dynamics and the Stokes shift obtained from the experiments. 92 What remains uncertain is exactly the connection between the large Stokes shift and the small fluorescence quantum yield of mPlum (10%).

The availability of multiple hydrogen bonding possibilities in the acylimine region appears to be a detriment to brightness. For example, TagRFP-675 (Figure 5b) was engineered from mKate to red shift the emission by introducing hydrogen bonding to the acylimine carbonyl, but these modifications resulted in a decrease in the fluorescence quantum yield (33% to 8%). Our time-resolved emission measurements revealed the presence of four emitting species of varying red shifts, which independently decay to the ground-state. Classical MD simulations also revealed multiple interconverting structures of

this hydrogen-bonding network, but it was not possible to assign the spectral forms to individual structures. <sup>15</sup> Interestingly, acylimine hydrogen bonding does not always lead to FPs with low fluorescence quantum yield. In developing the bright FusionRed mutant FR-MQV, we hypothesized that the M42Q mutation would be beneficial by occupying a cavity near the acylimine and thus locking it into a favorable geometry. This interaction increased the molecular brightness of the FP by 2-fold in comparison to FusionRed. It may be productive to focus attention on these issues using quantum and classical molecular simulations to examine models in which specific interactions with the chromophore is predicted to stabilize a single long-lived structure.

Electric Fields and Electrostatic Effects. Theoretical and experimental studies have examined the influence of electric fields and electrostatics on radiative and nonradiative rates. 45-47,61,81,95,97 For example, TD-DFT calculations on the isolated GFP chromophore (Figure 6) predict that electric fields can change the oscillator strength of an electronic transition and therefore the radiative rate constant. 96,97 Park and Rhee performed nonadiabatic molecular dynamics simulations on the GFP chromophore and found that electrostatic effects can outweigh steric factors impeding the twisting of the methine bridge between the phenoxy and imidazolinone rings, suppressing a major pathway for nonradiative relaxation.<sup>73</sup> Drobizhev and co-workers investigated these issues by measuring two-photon absorption cross sections of RFPs.<sup>57</sup> This cross-section is sensitive to the change in permanent dipole moment upon electronic excitation, which in part is controlled by the electric field on the chromophore. 57 They proposed that brighter fluorophores could be produced by fine-tuning the strength and

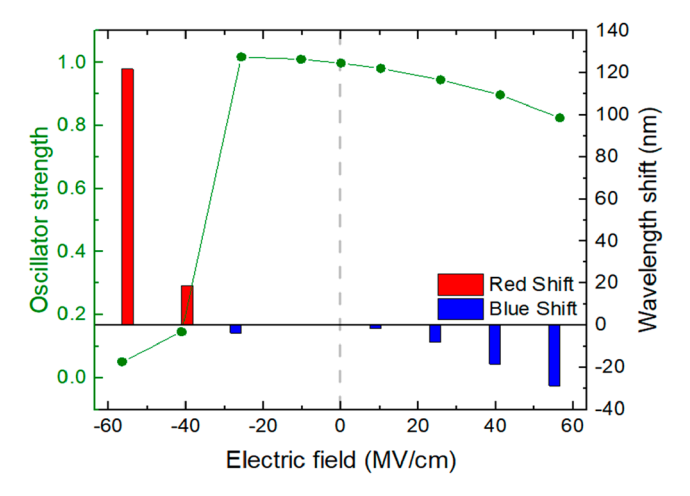


**Figure 6.** Graphical summary of results from a TD-DFT study performed by Kang et al., <sup>97</sup> which demonstrates that the oscillator strength and the absorption maxima for the GFP chromophore can be modulated with changes in the electric field.

directionality of the field, especially along the axis from the center of the imidazolinone ring to the phenolate ring. Electric fields along this axis are expected to change the amount of single bond vs double-bond character in the methine bridge, and therefore tune the rate of nonradiative decay associated with chromophore twisting followed by passage through a conical intersection to the ground state. Since this motion is accompanied by charge transfer across the methine bridge, the rate can be described by Marcus electron transfer theory. <sup>69</sup>

It is clearly a drastic oversimplification to characterize the electrostatic environment around the chromophore by specifying the electric field along different directions. In their tour de force 2019 publication,<sup>61</sup> Lin et al. circumvented this issue by treating the GFP absorption band as an intervalence charge transfer band between two resonance structures corresponding to the negative charge residing either on the phenolate oxygen or the carbonyl oxygen of the imidazolinone ring. The energetics of this charge transfer is described by Marcus-Hush theory. 98 The ground and excited state potential energy surfaces were described by coupling the diabatic electronic states for the two resonance forms through a bond-length alternation (BLA) coordinate. They demonstrate the electrondonating or electron withdrawing nature of the side chains at positions 203 and 96 (located at either end of the chromophore) controls the driving force for the charge transfer. This model quantitatively explains trends in absorption maxima, Stokes shifts, molar extinction coefficients, lineshapes, and other properties. For example, eliminating the Thr203 hydrogen bond with the phenolate oxygen reduces the driving force, leading to a decreased transition dipole moment, red-shifted absorption, a decreased Stokes shift, and a smaller vibronic sideband. The effect on the spectral line shape is due to the relative intensity of 0-0 and 0-1 vibronic peaks of the 1340 cm<sup>-1</sup> BLA mode, and occurs in addition to inhomogeneous broadening due to sensitivity of the electronic transition energy to an electric field. The theory can be applied to other chromoproteins such as photoactive yellow protein but it assumes the chromophore undergoes small geometry changes upon excitation and does not consider mutations that modify the electronic conjugation, so it does not explain the behavior of FPs such as BrUSLEE, where radiative rates are significantly modified by mutations. The model, however,

provides a significant physical insight for FP design, and it would be very useful to develop a similar approach which reduces the dimensionality of protein electrostatic effects to an energetic coordinate, for modeling other classes of FPs. With this, we move on to a discussion of FP photostability.

## 3. PHOTOSTABILITY

3.1. Photobleaching Measurements and Mechanisms. Irreversible photodamage or photobleaching is a hurdle to all applications. Despite the protection offered to the chromophore by encapsulation within the  $\beta$ -barrel, FPs generally photobleach faster than many small molecule fluorophores. This photoreactivity is possibly due to the diversity of chromophore interactions with the surrounding amino acid side chains and with freely diffusing species such as O2, which provide opportunities for photo-oxidation and electron-transfer reactions. 99 Identifying the mechanisms and/ or structures of the photobleached products has been a major challenge in FP development, most likely because several mechanisms are simultaneously at play and multiple products are formed. As a result, simple physical models have been of limited utility in guiding molecular design for higher photostability.

Photostability is influenced by the photophysics of the fluorophore and by the properties of the excitation source. A wide range of continuous wave (cw) or pulsed lasers, LEDs, and arc-lamps have been used for imaging and spectroscopic studies. Furthermore, in an attempt to investigate photobleaching under conditions corresponding to various imaging techniques, measurements have been performed with irradiances spanning several orders of magnitude, from  $\mu W/cm^2$  to kW/cm<sup>2</sup>. 100 Often, the decay of fluorescence intensity vs time is found to be nonexponential. As a result, the bleaching halflife is typically reported as a function of excitation irradiance. However, this half-life, or the corresponding average photobleaching rate, is highly dependent on the particular irradiation conditions such as the photon flux, excitation wavelength, peak intensity, and pulse duty cycle. 54,55 Furthermore, biochemical factors such as the buffer conditions for in vitro measurements, the host organism, and cellular localization (e.g., cytoplasmic, nuclear, or membrane-associated construct) are also important considerations. FPBase provides a note of caution for researchers interested in using posted values for comparing the photostability of different fluorophores.<sup>56</sup> The lack of standards for measuring and reporting photostability complicates decisions on which FP to select for a particular application and thus choices are often made on anecdotal evidence.

To address inconsistencies in reporting of photobleaching and other parameters, Cranfill et al. systematically measured the photobleaching and other properties of more than 40 FPs.  $^{100}$  A major revelation from their measurements is that the relationship between excitation intensity and photobleaching rates is typically supra-linear; i.e., the average photobleaching rate  $k_{bleach} \propto I^{\alpha}$  where  $\alpha > 1$  and is nearly quadratic for some FPs. For example, they found that mCherry emission decays with a half-life of 318 s when bleached with a 590 nm scanning-laser illumination at 80  $\mu{\rm W}$  excitation power vs 88 s when bleached with a 594 nm widefield LED source at 200  $\mu{\rm W}$  excitation power. Although this study represents a major step forward in characterizing FPs so that data-driven choices in experimental design can be made, the authors did not aim for a mechanistic understanding of photostability.

The lack of consistency in measuring and reporting photobleaching has posed challenges to creating models that connect photostability with other photophysical properties. To advance this field, we recommend that quantum yield of photobleaching ( $\Phi_{PB}$ ) be adopted as the gold standard for reporting and comparing FP photostability. Since, as discussed above, the power dependence of FP photobleaching may be nonlinear, and the value of  $\alpha$  might vary in different illumination regimes,  $\Phi_{PB}$  should be reported as a function of irradiance, similar to what is done for the 2-photon upconversion yields of lanthanide nanomaterials. This measure relies on normalizing the bleaching rates with excitation rates, which is determined by multiplying the irradiance on the sample with the absorption cross section at the excitation wavelength (eq 7).

$$\Phi_{PB}(I) = \frac{\text{number of molecules photolyzed}}{\text{number of photons absorbed}} = \frac{k_{bleaching}}{k_{excitation}}$$

$$= \frac{(\ln 2)N_{A}hc}{(2303)I \times \lambda \times \epsilon_{\lambda} \times t_{1/2bleaching}}$$
(7)

Here,  $N_A$  is Avogadro's constant, h is the Planck's constant, c is the speed of light, I is the irradiance (power per unit area),  $\lambda$  is the wavelength of excitation,  $\epsilon_{\lambda}$  is the extinction coefficient at  $\lambda$ , and  $t_{1/2bleaching}$  is the half-life obtained from the bleaching decay profile. Zak et al. followed this approach in considering the potential use of molecular fluorophores for luminescent convertors in LEDs. 102 According to their calculation, one of the most photostable dyes for laser spectroscopy, tetramethylrhodamine, has a  $\Phi_{PB}$  of 3.3  $\times$  10<sup>-7</sup>. Photostability data from FPBase suggest that the most stable FPs have  $\Phi_{PB}$  of  $\sim$ 10<sup>-4</sup> when analyzed with this approach.<sup>56</sup> Given that photon output before photobleaching limits the imaging duration and quality in many experiments, this 1000-fold difference in photostability between dyes and FPs indicates there is likely far more to be gained by improvements in photostability than in brightness.

The fluorescence profile is often found to decay on multiple time scales. The fastest time constant is typically associated with "reversible photobleaching," the same process which we already referred to as "dark state conversion," whereas the slower decay usually is due to permanent photobleaching. The relationship between the photobleaching rate constant and the half-life value is exact in the absence of dark-state conversion, and the photobleaching decay can be fit with a singleexponential. This relationship also applies in cases where the photobleaching is exponential and much slower than dark state conversion (e.g. EGFP and mScarlet). However, many FPs do exhibit long-lived dark states, and photoactivation or photoswitching processes compete with the first order kinetics of permanent photobleaching. Moreover, chromophores can permanently bleach from dark states. 103 Analogous dynamics are observed in azobenzene dyes, which like many FPs participate in a trans-cis isomerization under irradiation. 104 For azobenzenes, the dark cis conformer also bleaches without emitting, leading to nonlinearity of the photobleaching. We and others have reported methods for decoupling these processes from permanent photobleaching, and extracting the corresponding rate constants using other experiments such as fluorescence recovery measurements. 54,55,10

The brightest FPs often suffer from the highest photobleaching rates, in part because the photobleaching quantum yield is inversely proportional to the excited-state lifetime. For example, in the development of FR-MQV, as we selected for progressively longer fluorescence lifetime clones, we observed a trend toward shorter photobleaching half-life under excitation normalized widefield conditions (~5 W/cm²). FR-MQV has ~4-fold lower photostability than the parent FusionRed despite a 1.6-fold longer fluorescence lifetime.<sup>37</sup> Another example is mScarlet, which is 5-fold brighter than its variant mScarlet-H but has a 3-fold longer lifetime and a ~2-fold lower photostability (under 6.9 W/cm<sup>2</sup> widefield excitation and 1.35 W/cm<sup>2</sup> spinning-disk confocal excitation).<sup>34</sup> However, it is interesting to note that the drop in photostability does not scale exactly linearly with the increase in fluorescence lifetime for these two cases: it can be larger or smaller than expected. This observation suggests that different mechanisms of photobleaching may be at play within the two RFP families. More generally, examining the cases which deviate from the expected linear scaling within a closely related series of FPs might provide some insight into the structural features associated with photobleaching.

Turning to molecular mechanisms, computational and experimental studies suggest that photodamage is associated with the availability of molecular oxygen and diffusion of water molecules inside the  $\beta$ -barrel. <sup>99,106,107</sup> Excited electronic states have higher reduction potentials than the ground state and are therefore more susceptible to reacting with species such as  $^{1}O_{2}$ , which has been shown to be a major participant in photobleaching in certain cases. 99,106 Mechanistic investigations of phototoxic FPs that have found applications in chromophore-assisted light inactivation (CALI), have provided important insights into photobleaching. In these systems, photobleaching seems to be directed into one overall reaction. To understand this process, Grigorenko and co-workers employed QM/MM simulations to investigate the reactivity of the FP KillerRed. Their analysis revealed that a model excited-state FP chromophore can react with O2 through several possible charge transfer intermediates. By sampling many reaction pathways, their analysis identified a low activation barrier pathway (~13 kcal/mol) in which the hydroxyphenyl moiety is oxidized to a benzoquinone species that can diffuse out of the  $\beta$ -barrel. This result is consistent with electron density maps from an X-ray crystal structure of photobleached KillerRed. 108 Sen et al. recently performed QM/MM simulations to explore the role of T65/S65, the first chromophore-forming residue in EGFP and EYFP, respectively. For EGFP, a T65G substitution reduced the fluorescence lifetime but increased photostability, with a reduction of the characteristic green-to-red oxidative photoconversion, or "redding" behavior commonly observed for EGFP. 109 This phenomenon is observed when the GFP chromophore is oxidized to red-shifted absorption and emission species by high irradiance illumination. The transfer of fluorescing populations to such species has been linked to faster photobleaching. 110,111 We refer the reader to the work of Acharya et. al for a detailed explanation of this phenomenon.<sup>16</sup>

Dark states can also contribute to photobleaching. The lifetimes of triplet states, for example, are orders of magnitude longer than the  $S_1$  state and can, in fact, catalyze the formation of  $^1O_2$ , which greatly speeds up photochemistry promoting chromophore destruction.  $^{54,64}$  Therefore, reagents like oxygen scavengers and triplet-state quenchers are promising tools for slowing the rate of photobleaching, as they create apoxia in the system or depopulate nonfluorescent triplet states.  $^{112}$  Another

complication is that cases have been observed where the effect of dark states on photobleaching depends on the illumination conditions. For example, we found that the RFP mCherry was more photostable under pulsed illumination than under cw illumination, particularly at high irradiances (25 kW/cm²), suggesting that mCherry's dark state is photoreactive, whereas for the variant TagRFP R67K S158T, we found that the dark state is more photoprotective than photoreactive. <sup>54</sup>

3.2. Development of Photostable FPs. Despite these challenges, several studies have advanced fluorophore photostability. For example, single-cell phenotypic observation and tagging with light (SPOTlight), a cell sorting technique, led to the most stable yellow FP (YFP) observed to date, mGold. 113 In this case, eight libraries, each of 8000 variants were produced by targeted mutagenesis of 21 positions in the YFP mVenus (six near the chromophore) and expressed in yeast. SPOTlight then photobleached cells at an irradiance of  $\sim 2$ W/cm<sup>2</sup> and selected photostable variants from up to 700 000 cells in multiple rounds of selection. Similarly, high-throughput screening for photostable FPs using a Lego-based robot led the development of another YFP, Citrine2, which is ~2-fold more stable (in widefield and laser bleaching assays) than its precursor, mCitrine. 114 In this case, directed evolution of errorprone mutagenesis libraries was used with photostability selection with a 300 W white light xenon lamp source that had an effective white light irradiance of  $\sim 3.5 \text{ W/cm}^2$ . This study identified eight mutations that improved the photostability of Citrine2 in comparison to mCitrine but also led to unfavorable consequences such as dimerization and a drop in fluorescence lifetime from 3.6 to 3.3 ns. Surprisingly, these changes also led to a 5% increase in the radiative rate and 25% increase of the nonradiative rate. 114 These examples provide proof-of-principle demonstrations that screening large numbers of variants with new technologies can generate more photostable variants, but much more work remains to be done beyond the demonstration phase.

Our efforts to improve the photostability of mCherry using microfluidic technology led to the development of Kriek, which is 4-fold more photostable in confocal fluorescence microscopy. 107 This variant was selected from a 144 000member library designed with guidance from MD simulations. The simulations identified a region of the  $\beta$ -7/10 strand interface that showed ns-time scale fluctuations inconsistent with a rigid barrel structure, and we identified additional positions adjacent to this region which appeared tolerant to mutations. Selection was performed to minimize the amplitude of fluorescence signal lost after excitation from four sequential excitation beams (to mimic pulsed excitation in flow) under irradiance of  $\sim 2 \text{ kW/cm}^2$ . We later found that high irradiancepulsed excitation tends to populate dark states in mCherry and TagRFP variants. Since the microfluidic-based selection of Kriek was carried out with a similar excitation scheme, we also found that Kreik had lower rate constants for dark state conversion.<sup>54</sup> Previously, we demonstrated that the progenitor mCherry has a photoreactive dark state. Therefore, a reduction in the rate of dark state conversion may have resulted in an additional boost to the photostability of Kreik. Unfortunately, we observe a significant drop in the fluorescence quantum yield of Kriek (8%) with respect to the precursor mCherry (22%) with this strategy. The lesson here is that MD simulations can provide useful insight for library design, but that screening only on photobleaching is likely to produce variants with compromised brightness.

Other site-directed mutagenesis studies have been fruitful, as evident in the development of SiriusGFP-which is 2-fold more stable than its precursor EGFP and was found to be well suited for imaging at high irradiance (~kW/cm²) and long time-lapse imaging assays. 115 In this case, site-directed mutagenesis was guided by considering photochemical reactions of the model GFP chromophore. They found that S147R and S205V mutations in EGFP greatly enhanced the photostability under high irradiance laser-based imaging. 115,116 As with other efforts to improve photostability, SiriusGFP suffers from reduced brightness in comparison to EGFP due to an  $\sim$  3-fold reduction in its fluorescence quantum yield. When Ren et al. (2016) introduced a cysteine group near the chromophore of the RFP mKate2, it resulted in the 12-fold improved variant, "mStable." The photostability of mStable was attributed to the sulfoxidation of a cysteine residue facing the p-hydroxyphenyl moiety of the chromophore. Similar substitutions in mPlum resulted in a 23-fold stable variant. 117 The development of mGold from mVenus and Citrine2 from mCitrine, demonstrates that photostability can be improved without significant compromises in molecular brightness. This outcome suggests that it is possible to evolve existing bright FPs into more photostable variants, and vice versa, perhaps by screening libraries simultaneously on photostability and fluorescence lifetime.

Inspiration for FP design and applications may draw from effective techniques that minimize photobleaching in molecular fluorophores, such as utilizing triplet state quenchers and using systems that induce anoxia. <sup>118</sup> In addition, a promising strategy was recently reported where deuteration of small molecule dyes such as tetramethylrhodamine and JaneliaFluor (JF) dyes substantially improved photostability without causing detrimental changes to the electronic or photophysical properties. 119 For these types of dye molecules, alkylamine oxidation produces a distinctive secondary isotope effect, where deuteration of hydrogen atoms may reduce a twistedintermolecular charge transfer process, as is commonly observed for many FPs and in xanthene based JF dyes. Deuteration additionally increases the strength of the C-D bond and also affects the <sup>1</sup>O<sub>2</sub> oxidation rate, which manifests in higher (~1.2 fold) photostability. In addition to these molecular strategies, methods that involve the light source, such as control of photon statistics, pulse shaping, or excitation with squeezed light may also be promising tools for imaging FPs for longer periods of time by increasing the measurement precision attainable for a particular photon dose, even if these techniques do not directly reveal the chemistry behind photobleaching. 120

## 4. CONCLUSIONS

A few themes emerge when we consider the evolution of this field over the past 30 years. Initially, FP development relied on relatively straightforward structure-guided design and chemical intuition with screening on cellular brightness. As the productivity of this approach has started to decline, new variants have been introduced by relying on more advanced screening methods, with narrowly focused photophysical and biochemical goals. Our knowledge of FP structure and the diversity of their photophysics has dramatically expanded; however, at the same time, the pace of new FP development has slowed, e.g. of the more than 1500 FPs collected in FPbase, 270 were reported in the peak years of 2009–2010, decreasing to about half that number in subsequent two-year periods since

then. Is this slow-down due to the limits of our technology or of our insight? We think mostly the latter. How will the field continue to advance? Technology for faster, more precise screening of large libraries can partially make up for our knowledge gaps. Screening of RNA aptamer or protein libraries several orders of magnitude larger than those in FP development have frequently been used to successfully evolve high-affinity, specific ligand binding when physical insight is not applied to the library designs. Nevertheless, screening on complex functions such as photophysical properties will require more physical insight applied to the molecular design, and we feel that a renaissance of FP development might follow from investments in new experimental and theoretical approaches.

Experimental studies combining selections that go beyond "skimming the crème off the top" of libraries and simply keeping and studying the best clones could lead to unexpected insights. If the screening is performed such that the evolution of the properties and the structures within the libraries are monitored on a large scale, then bioinformatics and machinelearning techniques could be used to obtain more information about why some selections work and why some selections do not produce improvements. 123 Computational methods such as classical molecular dynamics and hybrid quantum-molecular mechanics would be valuable for creating models that advance our understanding of FP conformational dynamics and photoreactions such as photobleaching. These efforts should be accompanied by refinement of classical physical chemistry theories of, e.g., internal conversion so that it can be understood when we are facing issues particular to a small class of chromophores vs hitting fundamental physical limits. These investigations could help us develop protein design strategies that bridge structural measures such chromophore planarity and rigidity, with photophysical parameters such as fluorescence lifetime or dark-state conversion rates. Clearly, physical chemists could make fundamental contributions to the development of new fluorescent proteins or utilize the progress in this field to explore new avenues in chemistry. 124 Progress on these topics may have impacts on areas beyond bioimaging, such as solar-energy conversion materials, biohybrid LED lighting, and biophotonics such as display technologies.

## AUTHOR INFORMATION

## **Corresponding Author**

Ralph Jimenez — JILA, University of Colorado at Boulder and National Institute of Standards and Technology, Boulder, Colorado 80309, United States; Department of Chemistry, University of Colorado at Boulder, Boulder, Colorado 80309, United States; orcid.org/0000-0002-8989-405X; Email: rjimenez@jila.colorado.edu

## Author

Srijit Mukherjee – JILA, University of Colorado at Boulder and National Institute of Standards and Technology, Boulder, Colorado 80309, United States; Department of Chemistry, University of Colorado at Boulder, Boulder, Colorado 80309, United States

Complete contact information is available at: https://pubs.acs.org/10.1021/acs.jpcb.1c05629

## **Author Contributions**

The manuscript was written by S.M. and R.J.

#### Note:

The authors declare no competing financial interest.

## **Biographies**



Ralph Jimenez earned his bachelor's degree in chemistry at Cornell University, where he had an inspiring undergraduate research experience working for Paul Houston. He earned his Ph.D. in Physical Chemistry at the University of Chicago under the direction of Graham Fleming, investigating femtosecond solvation dynamics and ultrafast dynamics of photosynthetic light harvesting. He was a postdoc at the University of California, San Diego, with Kent Wilson, where he contributed to the development of laser-plasma based, ultrafast time-resolved x-ray diffraction. From 1998 to 2003, he was a senior Research Associate at the Scripps Research Institute, where he worked with Floyd Romesberg on a number of topics, including the use of ultrafast nonlinear spectroscopy to investigate antigenantibody interactions. In 2003, he joined the Quantum Physics Division of NIST and started his own research group at JILA. His research on the directed evolution of fluorescent proteins combines protein engineering with microfluidics technologies and ultrafast spectroscopy. Recently, his group has been exploring the potential for quantum measurement techniques to enhance the sensitivity and information content of molecular spectroscopy and imaging.



Srijit Mukherjee is a doctoral candidate in Physical Chemistry at JILA and the Department of Chemistry at the University of Colorado at Boulder. He graduated from the Indian Institute of Science Education and Research, Mohali (IISER-M) with a BS-MS dual degree majoring in Chemistry (2011–2016). At IISER, he was mentored by Kodumudi S. Viswanathan to study the mechanisms of energy transfer in ligand-sensitized fluorescence from lanthanide complexes. Subsequently, he completed his master's thesis under KSV's supervision on the conformational analysis and hydrogen-bonding of molecular complexes using *ab initio* calculations and matrixisolation IR spectroscopy. In the fall of 2016, he enrolled in the

graduate program at Boulder. He has been advised by Ralph Jimenez toward a dissertation focusing on the spectroscopic assessment and photophysical properties of red fluorescent proteins, with the goal of gaining molecular knowledge, studying pathways of excited state population decay, developing tools for engineering brighter fluorescent proteins, and directing potential applications of fluorescent probes in the context of biological imaging. His current research interests entail molecular biophysics, spectroscopy, photonics, optics-integrated microfluidics, and live-cell and single molecule fluorescence imaging.

## ACKNOWLEDGMENTS

S.M. was supported by the NIH/CU Molecular Biophysics Training Program (T32). This work was partially supported by the NSF Physics Frontier Center at JILA (PHY 1734006 to R.J.). We acknowledge the valuable contributions from Dr. Sheng-Ting Hung, Dr. Premashis Manna, Dr. Nancy Douglas, Pia Friis, Dr. Vlad Lychagov, Dr. Felix Vietmeyer, Dr. Kevin Dean, Dr. Josh Slocum, Dr. Patrick Konold, Dr. Brett Fiedler, Dr. Samantha Allen, Dr. Jennifer Lubbeck, and Prof. Lloyd Davis to the FP photophysics and development work in the Jimenez Lab. Finally, we have benefitted from many insightful discussions over the years with Prof. Amy Palmer and Prof. Prem Chapagain.

## REFERENCES

- (1) Shaner, N. C.; Steinbach, P. A.; Tsien, R. Y. A Guide to Choosing Fluorescent Proteins. *Nat. Methods* **2005**, 2 (12), 905–909. (2) Tsien, R. Y. The Green Fluorescent Protein. *Annu. Rev. Biochem.* **1998**, 67 (1), 509–544.
- (3) Duwé, S.; Dedecker, P. Optimizing the Fluorescent Protein Toolbox and Its Use. *Curr. Opin. Biotechnol.* **2019**, *58*, 183–191.
- (4) Algar, W. R.; Hildebrand, N.; Vogel, S. S.; Medintz, I. L. FRET as a Biomolecular Research Tool Understanding Its Potential While Avoiding Pitfalls. *Nat. Methods* **2019**, *16* (9), 815–829.
- (5) Coelho, S.; Poland, S. P.; Devauges, V.; Ameer-Beg, S. M. Adaptive Optics for a Time-Resolved Förster Resonance Energy Transfer (FRET) and Fluorescence Lifetime Imaging Microscopy (FLIM) in Vivo. *Opt. Lett.* **2020**, *45* (10), 2732.
- (6) Bando, Y.; Sakamoto, M.; Kim, S.; Ayzenshtat, I.; Yuste, R. Comparative Evaluation of Genetically Encoded Voltage Indicators. *Cell Reports* **2019**, 26 (3), 802–813.e4.
- (7) Tachibana, S. R.; Tang, L.; Zhu, L.; Liu, W.; Wang, Y.; Fang, C. Watching an Engineered Calcium Biosensor Glow: Altered Reaction Pathways before Emission. *J. Phys. Chem. B* **2018**, *122* (50), 11986–11005
- (8) Mo, H. M.; Xu, Y.; Yu, X. W. Improved Soluble Expression and Catalytic Activity of a Thermostable Esterase Using a High-Throughput Screening System Based on a Split-GFP Assembly. *J. Agric. Food Chem.* **2018**, *66* (48), 12756–12764.
- (9) Liu, Y.; Wolstenholme, C. H.; Carter, G. C.; Liu, H.; Hu, H.; Grainger, L. S.; Miao, K.; Fares, M.; Hoelzel, C. A.; Yennawar, H. P.; Ning, G.; Du, M.; Bai, L.; Li, X.; Zhang, X. Modulation of Fluorescent Protein Chromophores to Detect Protein Aggregation with Turn-On Fluorescence. *J. Am. Chem. Soc.* **2018**, *140* (24), 7381–7384.
- (10) Fernández-Luna, V.; Coto, P. B.; Costa, R. D. When Fluorescent Proteins Meet White Light-Emitting Diodes. *Angewandte Chemie International Edition* **2018**, *57*, 8826–8836.
- (11) Sigal, Y. M.; Zhou, R.; Zhuang, X. Visualizing and Discovering Cellular Structures with Super-Resolution Microscopy. *Science* **2018**, 361, 880–887.
- (12) Prasher, D. C.; Eckenrode, V. K.; Ward, W. W.; Prendergast, F. G.; Cormier, M. J. Primary Structure of the Aequorea Victoria Green-Fluorescent Protein. *Gene* **1992**, *111* (2), 229–233.
- (13) Prangsma, J. C.; Molenaar, R.; Van Weeren, L.; Bindels, D. S.; Haarbosch, L.; Stouthamer, J.; Gadella, T. W. J.; Subramaniam, V.;

- Vos, W. L.; Blum, C. Quantitative Determination of Dark Chromophore Population Explains the Apparent Low Quantum Yield of Red Fluorescent Proteins. *J. Phys. Chem. B* **2020**, *124* (8), 1383–1391.
- (14) Simine, L.; Lammert, H.; Sun, L.; Onuchic, J. N.; Rossky, P. J. Fluorescent Proteins Detect Host Structural Rearrangements via Electrostatic Mechanism. *J. Am. Chem. Soc.* **2018**, *140* (4), 1203–1206.
- (15) Konold, P. E.; Yoon, E.; Lee, J.; Allen, S. L.; Chapagain, P. P.; Gerstman, B. S.; Regmi, C. K.; Piatkevich, K. D.; Verkhusha, V. V.; Joo, T.; Jimenez, R. Fluorescence from Multiple Chromophore Hydrogen-Bonding States in the Far-Red Protein TagRFP675. *J. Phys. Chem. Lett.* **2016**, *7* (15), 3046–3051.
- (16) Acharya, A.; Bogdanov, A. M.; Grigorenko, B. L.; Bravaya, K. B.; Nemukhin, A. V.; Lukyanov, K. A.; Krylov, A. I. Photoinduced Chemistry in Fluorescent Proteins: Curse or Blessing? *Chem. Rev.* **2017**, *117*, 758–795.
- (17) Sen, T.; Ma, Y.; Polyakov, I. V.; Grigorenko, B. L.; Nemukhin, A. V.; Krylov, A. I. Interplay between Locally Excited and Charge Transfer States Governs the Photoswitching Mechanism in the Fluorescent Protein Dreiklang. *J. Phys. Chem. B* **2021**, *125* (3), 757–770
- (18) Bogdanov, A. M.; Acharya, A.; Titelmayer, A. V.; Mamontova, A. V.; Bravaya, K. B.; Kolomeisky, A. B.; Lukyanov, K. A.; Krylov, A. I. Turning on and off Photoinduced Electron Transfer in Fluorescent Proteins by  $\pi$ -Stacking, Halide Binding, and Tyr145 Mutations. *J. Am. Chem. Soc.* **2016**, *138* (14), 4807–4817.
- (19) Grigorenko, B. L.; Nemukhin, A. V.; Morozov, D. I.; Polyakov, I. V.; Bravaya, K. B.; Krylov, A. I. Toward Molecular-Level Characterization of Photoinduced Decarboxylation of the Green Fluorescent Protein: Accessibility of the Charge-Transfer States. *J. Chem. Theory Comput.* **2012**, *8* (6), 1912–1920.
- (20) Vegh, R. B.; Bravaya, K. B.; Bloch, D. A.; Bommarius, A. S.; Tolbert, L. M.; Verkhovsky, M.; Krylov, A. I.; Solntsev, K. M. Chromophore Photoreduction in Red Fluorescent Proteins Is Responsible for Bleaching and Phototoxicity. *J. Phys. Chem. B* **2014**, *118* (17), 4527–4534.
- (21) Kumagai, A.; Ando, R.; Miyatake, H.; Greimel, P.; Kobayashi, T.; Hirabayashi, Y.; Shimogori, T.; Miyawaki, A. XA Bilirubin-Inducible Fluorescent Protein from Eel Muscle. *Cell* **2013**, *153* (7), 1602
- (22) Rodriguez, E. A.; Tran, G. N.; Gross, L. A.; Crisp, J. L.; Shu, X.; Lin, J. Y.; Tsien, R. Y. A Far-Red Fluorescent Protein Evolved from a Cyanobacterial Phycobiliprotein. *Nat. Methods* **2016**, *13* (9), 763–769.
- (23) Shcherbakova, D. M.; Baloban, M.; Emelyanov, A. V.; Brenowitz, M.; Guo, P.; Verkhusha, V. V. Bright Monomeric Near-Infrared Fluorescent Proteins as Tags and Biosensors for Multiscale Imaging. *Nat. Commun.* **2016**, *7*, 12405.
- (24) Zhou, X. X.; Lin, M. Z. Photoswitchable Fluorescent Proteins: Ten Years of Colorful Chemistry and Exciting Applications. *Curr. Opin. Chem. Biol.* **2013**, *17*, 682–690.
- (25) Shcherbakova, D. M.; Sengupta, P.; Lippincott-Schwartz, J.; Verkhusha, V. V. Photocontrollable Fluorescent Proteins for Superresolution Imaging. *Annual Review of Biophysics* **2014**, 43 (1), 303–329.
- (26) ChemDraw, V. 20.1; PerkinElmer Informatics.
- (27) Humphrey, W.; Dalke, A.; Schulten, K. "VMD Visual Molecular Dynamics". J. Mol. Graphics 1996, 14, 33–38.
- (28) Balleza, E.; Kim, J. M.; Cluzel, P. Systematic Characterization of Maturation Time of Fluorescent Proteins in Living Cells. *Nat. Methods* **2018**, *15* (1), 47–51.
- (29) Manna, P.; Hung, S. T.; Mukherjee, S.; Friis, P.; Simpson, D. M.; Lo, M. N.; Palmer, A. E.; Jimenez, R. Directed Evolution of Excited State Lifetime and Brightness in FusionRed Using a Microfluidic Sorter. *Integrative Biology (United Kingdom)* **2018**, *10* (9), 516–526.

- (30) Cormack, B. P.; Valdivia, R. H.; Falkow, S. FACS-Optimized Mutants of the Green Fluorescent Protein (GFP). *Gene* 1996, 173, 33–38.
- (31) Kredel, S.; Oswald, F.; Nienhaus, K.; Deuschle, K.; Röcker, C.; Wolff, M.; Heilker, R.; Nienhaus, G. U.; Wiedenmann, J. mRuby, a Bright Monomeric Red Fluorescent Protein for Labeling of Subcellular Structures. *PLoS One* **2009**, *4* (2), e4391.
- (32) Shaner, N. C.; Lambert, G. G.; Chammas, A.; Ni, Y.; Cranfill, P. J.; Baird, M. A.; Sell, B. R.; Allen, J. R.; Day, R. N.; Israelsson, M.; Davidson, M. W.; Wang, J. A Bright Monomeric Green Fluorescent Protein Derived from Branchiostoma Lanceolatum. *Nat. Methods* **2013**, *10* (5), 407–409.
- (33) Grimm, J. B.; Tkachuk, A. N.; Xie, L.; Choi, H.; Mohar, B.; Falco, N.; Schaefer, K.; Patel, R.; Zheng, Q.; Liu, Z.; Lippincott-Schwartz, J.; Brown, T. A.; Lavis, L. D. A General Method to Optimize and Functionalize Red-Shifted Rhodamine Dyes. *Nat. Methods* **2020**, *17* (8), 815–821.
- (34) Bindels, D. S.; Haarbosch, L.; Van Weeren, L.; Postma, M.; Wiese, K. E.; Mastop, M.; Aumonier, S.; Gotthard, G.; Royant, A.; Hink, M. A.; Gadella, T. W. J. mScarlet: A Bright Monomeric Red Fluorescent Protein for Cellular Imaging. *Nat. Methods* **2017**, *14* (1), 53–56.
- (35) Lambert, G. G.; Depernet, H.; Gotthard, G.; Schultz, D. T.; Navizet, I.; Lambert, T.; Adams, S. R.; Torreblanca-Zanca, A.; Chu, M.; Bindels, D. S.; Levesque, V.; Nero Moffatt, J.; Salih, A.; Royant, A.; Shaner, N. C. Aequorea's Secrets Revealed: New Fluorescent Proteins with Unique Properties for Bioimaging and Biosensing. *PLoS Biology* **2020**, *18* (11), e3000936.
- (36) Campbell, B. C.; Nabel, E. M.; Murdock, M. H.; Lao-Peregrin, C.; Tsoulfas, P.; Blackmore, M. G.; Lee, F. S.; Liston, C.; Morishita, H.; Petsko, G. A. mGreenLantern: A Bright Monomeric Fluorescent Protein with Rapid Expression and Cell Filling Properties for Neuronal Imaging. *Proc. Natl. Acad. Sci. U.S.A.* **2020**, *117* (48), 30710–30721.
- (37) Mukherjee, S.; Hung, S. T.; Douglas, N.; Manna, P.; Thomas, C.; Ekrem, A.; Palmer, A. E.; Jimenez, R. Engineering of a Brighter Variant of the Fusionred Fluorescent Protein Using Lifetime Flow Cytometry and Structure-Guided Mutations. *Biochemistry* **2020**, *59* (39), 3669–3682.
- (38) Bindels, D. S.; Postma, M.; Haarbosch, L.; van Weeren, L.; Gadella, T. W. J. Multiparameter Screening Method for Developing Optimized Red-Fluorescent Proteins. *Nat. Protoc.* **2020**, *15* (2), 450–478.
- (39) Dean, K. M.; Davis, L. M.; Lubbeck, J. L.; Manna, P.; Friis, P.; Palmer, A. E.; Jimenez, R. High- Speed Multiparameter Photophysical Analyses of Fluorophore Libraries. *Anal. Chem.* **2015**, *87* (10), 5026–5030.
- (40) Hung, S. T.; Mukherjee, S.; Jimenez, R. Enrichment of Rare Events Using a Multi-Parameter High Throughput Microfluidic Droplet Sorter. *Lab Chip* **2020**, *20* (4), 834–843.
- (41) Lubbeck, J. L.; Dean, K. M.; Ma, H.; Palmer, A. E.; Jimenez, R. Microfluidic Flow Cytometer for Quantifying Photobleaching of Fluorescent Proteins in Cells. *Anal. Chem.* **2012**, *84* (9), 3929–3937.
- (42) Davis, L. M.; Lubbeck, J. L.; Dean, K. M.; Palmer, A. E.; Jimenez, R. Microfluidic Cell Sorter for Use in Developing Red Fluorescent Proteins with Improved Photostability. *Lab Chip* **2013**, 13 (12), 2320–2327.
- (43) Lychagov, V. V.; Shemetov, A. A.; Jimenez, R.; Verkhusha, V. V. Microfluidic System for In-Flow Reversible Photoswitching of near-Infrared Fluorescent Proteins. *Anal. Chem.* **2016**, *88* (23), 11821–11829
- (44) Zheng, L.; Migliore, A.; Beratan, D. N. Electrostatic Field-Induced Oscillator Strength Focusing in Molecules. *J. Phys. Chem. B* **2020**, 124 (29), 6376–6388.
- (45) Drobizhev, M.; Callis, P. R.; Nifosì, R.; Wicks, G.; Stoltzfus, C.; Barnett, L.; Hughes, T. E.; Sullivan, P.; Rebane, A. Long-and Short-Range Electrostatic Fields in GFP Mutants: Implications for Spectral Tuning. *Sci. Rep.* **2015**, *5*, 13223.

- (46) Myšková, J.; Rybakova, O.; Brynda, J.; Khoroshyy, P.; Bondar, A.; Lazar, J. Directionality of Light Absorption and Emission in Representative Fluorescent Proteins. *Proc. Natl. Acad. Sci. U.S.A.* **2020**, *117* (51), 32395–32401.
- (47) Molina, R. S.; King, J.; Franklin, J.; Clack, N.; McRaven, C.; Goncharov, V.; Flickinger, D.; Svoboda, K.; Drobizhev, M.; Hughes, T. E. High Throughput Instrument to Screen Fluorescent Proteins under Two-Photon Excitation. *Biomedical Optics Express* **2020**, *11* (12), 7192.
- (48) Mo, G. C. H.; Ross, B.; Hertel, F.; Manna, P.; Yang, X.; Greenwald, E.; Booth, C.; Plummer, A. M.; Tenner, B.; Chen, Z.; Wang, Y.; Kennedy, E. J.; Cole, P. A.; Fleming, K. G.; Palmer, A.; Jimenez, R.; Xiao, J.; Dedecker, P.; Zhang, J. Genetically Encoded Biosensors for Visualizing Live-Cell Biochemical Activity at Super-Resolution. *Nat. Methods* **2017**, *14* (4), 427–434.
- (49) Mo, G. C. H.; Posner, C.; Rodriguez, E. A.; Sun, T.; Zhang, J. A Rationally Enhanced Red Fluorescent Protein Expands the Utility of FRET Biosensors. *Nat. Commun.* **2020**, *11* (1), 1848.
- (50) Mohr, M. A.; Kobitski, A. Y.; Sabater, L. R.; Nienhaus, K.; Obara, C. J.; Lippincott-Schwartz, J.; Nienhaus, G. U.; Pantazis, P. Rational Engineering of Photoconvertible Fluorescent Proteins for Dual- Color Fluorescence Nanoscopy Enabled by a Triplet-State Mechanism of Primed Conversion. *Angew. Chem.* **2017**, *129*, 11786.
- (51) Li, M. J.; Lin, Y. H.; Sung, R.; Sung, K. E-Z Isomerization Mechanism of the Green Fluorescent Protein Chromophore: Remote Regulation by Proton Dissociation of the Phenol Group. *J. Phys. Chem. A* **2021**, *125* (17), 3614–3621.
- (52) Subach, F. V.; Verkhusha, V. V. Chromophore Transformations in Red Fluorescent Proteins. *Chem. Rev.* **2012**, *112*, 4308–4327.
- (53) Ruhlandt, D.; Andresen, M.; Jensen, N.; Gregor, I.; Jakobs, S.; Enderlein, J.; Chizhik, A. I. Absolute Quantum Yield Measurements of Fluorescent Proteins Using a Plasmonic Nanocavity. *Communications Biology* **2020**, *3* (1), 1–7.
- (54) Dean, K. M.; Lubbeck, J. L.; Binder, J. K.; Schwall, L. R.; Jimenez, R.; Palmer, A. E. Analysis of Red-Fluorescent Proteins Provides Insight into Dark-State Conversion and Photodegradation. *Biophys. J.* **2011**, *101* (4), 961–969.
- (55) Manna, P.; Jimenez, R. Time and Frequency-Domain Measurement of Ground-State Recovery Times in Red Fluorescent Proteins. J. Phys. Chem. B 2015, 119 (15), 4944–4954.
- (56) Lambert, T. J. FPbase: A Community-Editable Fluorescent Protein Database. *Nat. Methods* **2019**, *16*, 277–278.
- (57) Drobizhev, M.; Molina, R. S.; Callis, P. R.; Scott, J. N.; Lambert, G. G.; Salih, A.; Shaner, N. C.; Hughes, T. E. Local Electric Field Controls Fluorescence Quantum Yield of Red and Far-Red Fluorescent Proteins. *Frontiers in Molecular Biosciences* **2021**, *8*, 633217.
- (58) Mamontova, A. V.; Solovyev, I. D.; Savitsky, A. P.; Shakhov, A.; Lukyanov, K. A.; Bogdanov, A. M. Bright GFP with Subnanosecond Fluorescence Lifetime. *Sci. Rep.* **2018**, 8 (1), 13224.
- (59) Strickler, S. J.; Berg, R. A. Relationship between Absorption Intensity and Fluorescence Lifetime of Molecules. *J. Chem. Phys.* **1962**, 37 (4), 814–822.
- (60) Jung, G.; Brockhinke, A.; Gensch, T.; Hötzer, B.; Schwedler, S.; Veettil, S. K. Fluorescence Lifetime of Fluorescent Proteins. In *Fluorescent Proteins I: From Understanding to Design*; Jung, G., Ed.; Springer: Berlin and Heidelberg, Germany, 2011; pp 69–97;
- (61) Lin, C. Y.; Romei, M. G.; Oltrogge, L. M.; Mathews, I. I.; Boxer, S. G. Unified Model for Photophysical and Electro-Optical Properties of Green Fluorescent Proteins. *J. Am. Chem. Soc.* **2019**, *141* (38), 15250–15265.
- (62) Terazono, H.; Anzai, Y.; Soloviev, M.; Yasuda, K. Labelling of live cells using fluorescent aptamers: Binding reversal with DNA nucleases. *J. Nanobiotechnol.* **2010**, *8*, 8.
- (63) Tregidgo, C.; Levitt, J. A.; Suhling, K. Effect of refractive index on the fluorescence lifetime of green fluorescent protein. *Journal of Biomedical Optics* **2008**, *13* (3), No. 031218.
- (64) Byrdin, B.; Duan, C.; Bourgeois, D.; Brettel, K. A Long-Lived Triplet State Is the Entrance Gateway to Oxidative Photochemistry in

- Green Fluorescent Proteins. J. Am. Chem. Soc. 2018, 140 (8), 2897–2905.
- (65) Canty, L.; Hariharan, S.; Liu, Q.; Haney, S. A.; Andrews, D. W. Peak emission wavelength and fluorescence lifetime are coupled in far-red, GFP-like fluorescent proteins. *PLoS One* **2018**, *13* (11), No. e0208075.
- (66) Mauring, K.; Krasnenko, V.; Miller, S. Photophysics of the blue fluorescent protein. *J. Lumin.* **2007**, *122–123* (1–2), 291–293.
- (67) Bhalekar, S. B.; Bhagwat, A. A.; Sekar, N. Orange-Red Fluorescent (Partially Rigidified) Donor-π-(rigidified)-Acceptor System Computational Studies. *J. Fluoresc.* **2020**, 30 (3), 565–579.
- (68) Englman, R.; Jortner, J. The Energy Gap Law for Radiationless Transitions in Large Molecules. *Mol. Phys.* **1970**, *18* (2), 145.
- (69) Marcus, R. A. On the theory of oxidation-reduction reactions involving electron transfer. I. J. Chem. Phys. 1956, 24 (5), 966–978.
- (70) Fleming, G. R.; Cho, M. Chromophore-solvent dynamics. *Annu. Rev. Phys. Chem.* **1996**, 47 (1), 109–134.
- (71) Jordanides, X. J.; Lang, M. J.; Song, X.; Fleming, G. R. Solvation dynamics in protein environments studied by photon echo spectroscopy. *J. Phys. Chem. B* **1999**, *103* (37), 7995–8005.
- (72) Jimenez, R.; Salazar, G.; Yin, J.; Joo, T.; Romesberg, F. E. Protein dynamics and the immunological evolution of molecular recognition. *Proc. Natl. Acad. Sci. U.S.A.* **2004**, *101* (11), 3803–3808.
- (73) Park, J. W.; Rhee, Y. M. Electric Field Keeps Chromophore Planar and Produces High Yield Fluorescence in Green Fluorescent Protein. *J. Am. Chem. Soc.* **2016**, 138 (41), 13619–13629.
- (74) Bravaya, K. B.; Grigorenko, B. L.; Nemukhin, A. V.; Krylov, A. I. Quantum Chemistry behind Bioimaging: Insights from Ab Initio Studies of Fluorescent Proteins and Their Chromophores. *Accounts of chemical research* **2012**, 45 (2), 265–275.
- (75) Shu, X.; Shaner, N. C.; Yarbrough, C. A.; Tsien, R. Y.; Remington, S. J. Novel Chromophores and Buried Charges Control Color in mFruits. *Biochemistry* **2006**, *45* (32), 9639–9647.
- (76) Goedhart, J.; Von Stetten, D.; Noirclerc-Savoye, M.; Lelimousin, M.; Joosen, L.; Hink, M. A.; Van Weeren, L.; Gadella, T. W. J.; Royant, A. Structure-Guided Evolution of Cyan Fluorescent Proteins towards a Quantum Yield of 93%. *Nat. Commun.* **2012**, *3*, 751
- (77) Conyard, J.; Heisler, I. A.; Chan, Y.; Bulman Page, P. C.; Meech, S. R.; Blancafort, L. A New Twist in the Photophysics of the GFP Chromophore: A Volume-Conserving Molecular Torsion Couple. *Chemical Science* **2018**, 9 (7), 1803–1812.
- (78) Konold, P.; Regmi, C. K.; Chapagain, P. P.; Gerstman, B. S.; Jimenez, R. Hydrogen Bond Flexibility Correlates with Stokes Shift in mPlum Variants. *J. Phys. Chem. B* **2014**, *118* (11), 2940–2948.
- (79) Steiert, F.; Petrov, E. P.; Schultz, P.; Schwille, P.; Weidemann, T. Photophysical Behavior of MNeonGreen, an Evolutionarily Distant Green Fluorescent Protein. *Biophys. J.* **2018**, *114* (10), 2419–2431.
- (80) Tao, A.; Zhang, R.; Yuan, J. Characterization of Photophysical Properties of Photoactivatable Fluorescent Proteins for Super-Resolution Microscopy. *J. Phys. Chem. B* **2020**, *124* (10), 1892–1897.
- (81) Romei, M. G.; Lin, C. Y.; Mathews, I. I.; Boxer, S. G. Electrostatic Control of Photoisomerization Pathways in Proteins. *Science* **2020**, *367* (6473), 76–79.
- (82) Coquelle, N.; Sliwa, M.; Woodhouse, J.; Schirò, G.; Adam, V.; Aquila, A.; Barends, T. R. M.; Boutet, S.; Byrdin, M.; Carbajo, S.; De la Mora, E.; Doak, R. B.; Feliks, M.; Fieschi, F.; Foucar, L.; Guillon, V.; Hilpert, M.; Hunter, M. S.; Jakobs, S.; Koglin, J. E.; Kovacsova, G.; Lane, T. J.; Lévy, B.; Liang, M.; Nass, K.; Ridard, J.; Robinson, J. S.; Roome, C. M.; Ruckebusch, C.; Seaberg, M.; Thepaut, M.; Cammarata, M.; Demachy, I.; Field, M.; Shoeman, R. L.; Bourgeois, D.; Colletier, J. P.; Schlichting, I.; Weik, M. Chromophore Twisting in the Excited State of a Photoswitchable Fluorescent Protein Captured by Time-Resolved Serial Femtosecond Crystallography. *Nat. Chem.* 2018, 10 (1), 31–37.
- (83) Laptenok, S. P.; Gil, A. A.; Hall, C. R.; Lukacs, A.; Iuliano, J. N.; Jones, G. A.; Greetham, G. M.; Donaldson, P.; Miyawaki, A.; Tonge, P. J.; Meech, S. R. Infrared Spectroscopy Reveals Multi-Step Multi-

- Timescale Photoactivation in the Photoconvertible Protein Archetype Dronpa. *Nat. Chem.* **2018**, *10* (8), 845–852.
- (84) Mizuno, H.; Mal, T. K.; Wälchli, M.; Kikuchi, A.; Fukano, T.; Ando, R.; Jeyakanthan, J.; Taka, J.; Shiro, Y.; Ikura, M.; Miyawaki, A. Light-Dependent Regulation of Structural Flexibility in a Photochromic Fluorescent Protein. *Proc. Natl. Acad. Sci. U.S.A.* **2008**, *105* (27), 9227–9232.
- (85) Oscar, B. G.; Zhu, L.; Wolfendeen, H.; Rozanov, N. D.; Chang, A.; Stout, K. T.; Sandwisch, J. W.; Porter, J. J.; Mehl, R. A.; Fang, C. Dissecting Optical Response and Molecular Structure of Fluorescent Proteins with Non-Canonical Chromophores. *Frontiers in Molecular Biosciences* **2020**, 7 (July), 1–10.
- (86) Widder, P.; Schuck, J.; Summerer, D.; Drescher, M. Combining Site-Directed Spin Labeling: In Vivo and in-Cell EPR Distance Determination. *Phys. Chem. Chem. Phys.* **2020**, 22 (9), 4875–4879.
- (87) Christou, N. E.; Ayala, I.; Giandoreggio-Barranco, K.; Byrdin, M.; Adam, V.; Bourgeois, D.; Brutscher, B. NMR Reveals Light-Induced Changes in the Dynamics of a Photoswitchable Fluorescent Protein. *Biophys. J.* **2019**, *117* (11), 2087–2100.
- (88) Bourgeois, D. Deciphering Structural Photophysics of Fluorescent Proteins by Kinetic Crystallography. *International Journal of Molecular Sciences.* **2017**, *18*, 1187.
- (89) De Zitter, E.; Thédié, D.; Mönkemöller, V.; Hugelier, S.; Beaudouin, J.; Adam, V.; Byrdin, M.; Van Meervelt, L.; Dedecker, P.; Bourgeois, D. Mechanistic Investigation of MEos4b Reveals a Strategy to Reduce Track Interruptions in SptPALM. *Nat. Methods* **2019**, *16* (8), 707–710.
- (90) Yoon, E.; Konold, P. E.; Lee, J.; Joo, T.; Jimenez, R. Far-Red Emission of mPlum Fluorescent Protein Results from Excited-State Interconversion between Chromophore Hydrogen-Bonding States. J. Phys. Chem. Lett. 2016, 7 (12), 2170–2174.
- (91) Moron, V.; Marazzi, M.; Wanko, M. Far Red Fluorescent Proteins: Where Is the Limit of the Acylimine Chromophore? *J. Chem. Theory Comput.* **2019**, 15 (7), 4228–4240.
- (92) Faraji, S.; Krylov, A. I. On the Nature of an Extended Stokes Shift in the mPlum Fluorescent Protein. *J. Phys. Chem. B* **2015**, *119* (41), 13052–13062.
- (93) Abbyad, P.; Childs, W.; Shi, X.; Boxer, S. G. Dynamic Stokes Shift in Green Fluorescent Protein Variants. *Proc. Natl. Acad. Sci. U.S.A.* **2007**, *104* (51), 20189–20194.
- (94) Piatkevich, K. D.; Malashkevich, V. N.; Morozova, K. S.; Nemkovich, N. A.; Almo, S. C.; Verkhusha, V. V. Extended Stokes Shift in Fluorescent Proteins: Chromophore-Protein Interactions in a near- Infrared TagRFP675 Variant. *Sci. Rep.* **2013**, *3*, 1847.
- (95) Khrenova, M. G.; Mulashkin, F. D.; Bulavko, E. S.; Zakharova, T. M.; Nemukhin, A. V. Dipole Moment Variation Clears up Electronic Excitations in the  $\pi$ -Stacked Complexes of Fluorescent Protein Chromophores. *J. Chem. Inf. Model.* **2020**, 60 (12), 6288–6297
- (96) Kang, B.; Liu, H.; Jang, D. J.; Lee, J. Y. Electric Field Effect on the Ground State Proton Transfer in the H-Bonded HBDI Complex: An Implication of the Green Fluorescent Protein. *RSC Adv.* **2014**, *4* (51), 26543–26551.
- (97) Kang, B.; Baek, K. Y.; Lee, J. Y. Electric Field Effect on Trans-p-Hydroxybenzylideneimidazolidinone: A DFT Study and Implication to Green Fluorescent Protein. *Bulletin of the Korean Chemical Society* **2015**, 36 (1), 276–281.
- (98) Treynor, T. P.; Andrews, S. S.; Boxer, S. G. Intervalence band stark effect of the special pair radical cation in bacterial photosynthetic reaction centers. *J. Phys. Chem. B* **2003**, *107* (40), 11230–11239.
- (99) Grigorenko, B. L.; Nemukhin, A. V.; Polyakov, I. V.; Khrenova, M. G.; Krylov, A. I. A Light-Induced Reaction with Oxygen Leads to Chromophore Decomposition and Irreversible Photobleaching in GFP-Type Proteins. *J. Phys. Chem. B* **2015**, *119*, 5444.
- (100) Cranfill, P. J.; Sell, B. R.; Baird, M. A.; Allen, J. R.; Lavagnino, Z.; De Gruiter, H. M.; Kremers, G. J.; Davidson, M. W.; Ustione, A.; Piston, D. W. Quantitative Assessment of Fluorescent Proteins. *Nat. Methods* **2016**, *13* (7), 557–562.

- (101) Meijer, M. S.; Rojas-Gutierrez, P. A.; Busko, D.; Howard, I. A.; Frenzel, F.; Würth, C.; Resch-Genger, U.; Richards, B. S.; Turshatov, A.; Capobianco, J. A.; Bonnet, S. Absolute upconversion quantum yields of blue-emitting LiYF4:Yb3+, Tm3+ upconverting nanoparticles. *Phys. Chem. Chem. Phys.* **2018**, 20 (35), 22556–22562.
- (102) Zak, P. P.; Lapina, V. A.; Pavich, T. A.; Trofimov, A. V.; Trofimova, N. N.; Tsaplev, Y. B. Luminescent Materials for Modern Light Sources. *Russ. Chem. Rev.* **2017**, *86* (9), 831–844.
- (103) Widengren, J.; Rigler, R. Mechanisms of photobleaching investigated by fluorescence correlation spectroscopy. *Bioimaging* **1996**, *4* (3), 149–157.
- (104) Serra, F.; Terentjev, E. M. Nonlinear dynamics of absorption and photobleaching of dyes. *J. Chem. Phys.* **2008**, *128* (22), 224510. (105) Lew, M. D.; Lee, S. F.; Ptacin, J. L.; Lee, M. K.; Twieg, R. J.; Shapiro, L.; Moerner, W. E. Three-dimensional superresolution colocalization of intracellular protein superstructures and the cell surface in live Caulobacter crescentus. *Proc. Natl. Acad. Sci. U.S.A.* **2011**, *108* (46), E1102—E1110.
- (106) Demchenko, A. P. Photobleaching of Organic Fluorophores: Quantitative Characterization, Mechanisms, Protection. *Methods and Applications in Fluorescence* **2020**, *8*, 022001.
- (107) Dean, K. M.; Lubbeck, J. L.; Davis, L. M.; Regmi, C. K.; Chapagain, P. P.; Gerstman, B. S.; Jimenez, R.; Palmer, A. E. Microfluidics-Based Selection of Red-Fluorescent Proteins with Decreased Rates of Photobleaching. *Integrative Biology (United Kingdom)* 2015, 7 (2), 263–273.
- (108) Bulina, M. E.; Lukyanov, K. A.; Britanova, O. V.; Onichtchouk, D.; Lukyanov, S.; Chudakov, D. M. Chromophore-Assisted Light Inactivation (CALI) Using the Phototoxic Fluorescent Protein KillerRed. *Nat. Protoc.* **2006**, *1* (2), 947–953.
- (109) Sen, T.; Mamontova, A. V.; Titelmayer, A. V.; Shakhov, A. M.; Astafiev, A. A.; Acharya, A.; Lukyanov, K. A.; Krylov, A. I.; Bogdanov, A. M. Influence of the First Chromophore-Forming Residue on Photobleaching and Oxidative Photoconversion of EGFP and EYFP. *International Journal of Molecular Sciences* **2019**, 20 (20), 5229.
- (110) Bogdanov, A. M.; Bogdanova, E. A.; Chudakov, D. M.; Gorodnicheva, T. V.; Lukyanov, S.; Lukyanov, K. A. Cell Culture Medium Affects GFP Photostability: A Solution. *Nat. Methods* **2009**, *6*, 859–860.
- (111) Gorbachev, D. A.; Petrusevich, E. F.; Kabylda, A. M.; Maksimov, E. G.; Lukyanov, K. A.; Bogdanov, A. M.; Baranov, M. S.; Bochenkova, A. V.; Mishin, A. S. A General Mechanism of Green-to-Red Photoconversions of GFP. *Frontiers in Molecular Biosciences* **2020**, 7, 00176.
- (112) Kwon, J.; Park, J. S.; Kang, M.; Choi, S.; Park, J.; Kim, G. T.; Lee, C.; Cha, S.; Rhee, H. W.; Shim, S. H. Bright Ligand-Activatable Fluorescent Protein for High-Quality Multicolor Live-Cell Super-Resolution Microscopy. *Nat. Commun.* **2020**, *11*, 273.
- (113) Lee, J.; Liu, Z.; Suzuki, P. H.; Ahrens, J. F.; Lai, S.; Lu, X.; Guan, S.; St-Pierre, F. Versatile Phenotype-Activated Cell Sorting. *Sci. Adv.* **2020**, *6* (43), 1–18.
- (114) Wiens, M. D.; Hoffmann, F.; Chen, Y.; Campbell, R. E. Enhancing Fluorescent Protein Photostability through Robot-Assisted Photobleaching. *Integrative Biology (United Kingdom)* **2018**, *10* (7), 419–428.
- (115) Zhong, S.; Rivera-Molina, F.; Rivetta, A.; Toomre, D.; Santos-Sacchi, J.; Navaratnam, D. Seeing the Long Tail: A Novel Green Fluorescent Protein, SiriusGFP, for Ultra Long Timelapse Imaging. *Journal of Neuroscience Methods* **2019**, *313*, 68–76.
- (116) Chatterjee, T.; Mandal, M.; Gude, V.; Bag, P. P.; Mandal, P. K. Strong Electron Donation Induced Differential Nonradiative Decay Pathways for Para and Meta GFP Chromophore Analogues. *Phys. Chem. Chem. Phys.* **2015**, *17* (32), 20515–20521.
- (117) Ren, H.; Yang, B.; Ma, C.; Hu, Y. S.; Wang, P. G.; Wang, L. Cysteine Sulfoxidation Increases the Photostability of Red Fluorescent Proteins. ACS Chem. Biol. 2016, 11 (10), 2679–2684.
- (118) Nahidiazar, L.; Agronskaia, A. V.; Broertjes, J.; Van den Broek, B.; Jalink, K. Optimizing Imaging Conditions for Demanding Multi-

- Color Super Resolution Localization Microscopy. PLoS One 2016, 11 (7), e0158884.
- (119) Grimm, J. B.; Xie, L.; Casler, J. C.; Patel, R.; Tkachuk, A. N.; Choi, H.; Lippincott-Schwartz, J.; Brown, T. A.; Glick, B. S.; Liu, Z.; Lavis, L. D. Deuteration Improves Small-Molecule Fluorophores. bioRxiv. 2020; DOI: 10.1101/2020.08.17.250027.
- (120) Parzuchowski, K. M.; Mikhaylov, A.; Mazurek, M. D.; Wilson, R. N.; Lum, D. J.; Gerrits, T.; Camp, C. H.; Stevens, M. J.; Jimenez, R. Setting Bounds on Two-Photon Absorption Cross-Sections in Common Fluorophores with Entangled Photon Pair Excitation. *Physical Review Applied* **2021**, *15* (4), 044012.
- (121) Kay, B. K., Winter, J., McCafferty, J. B., Eds. Front Matter. In *Phage Display of Peptides and Proteins*; Academic Press: 1996; p iii; DOI: 10.1016/b978-0-12-402380-2.50023-x.
- (122) Ellington, A. D.; Szostak, J. W. In vitro selection of RNA molecules that bind specific ligands. *Nature* **1990**, 346 (6287), 818–822
- (123) Sarkisyan, K. S.; Bolotin, D. A.; Meer, M. V.; Usmanova, D. R.; Mishin, A. S.; Sharonov, G. V.; Ivankov, D. N.; Bozhanova, N. G.; Baranov, M. S.; Soylemez, O.; Bogatyreva, N. S.; Vlasov, P. K.; Egorov, E. S.; Logacheva, M. D.; Kondrashov, A. S.; Chudakov, D. M.; Putintseva, E. V.; Mamedov, I. Z.; Tawfik, D. S.; Lukyanov, K. A.; Kondrashov, F. A. Local fitness landscape of the green fluorescent protein. *Nature* **2016**, *533*, *397*–401.
- (124) Lin, C.-Y.; Romei, M.; Mathews, I.; Boxer, S. Energetic Basis of Excited-State Enzyme Design and Function. *ChemRxiv* 2021; DOI: 10.33774/chemrxiv-2021-9l2vn-v2.

## **□** Recommended by ACS

## Fluorescence Modulation by Ultrafast Chromophore Twisting Events: Developing a Powerful Toolset for Fluorescent-Protein-Based Imaging

Longteng Tang and Chong Fang

DECEMBER 09, 2021

THE JOURNAL OF PHYSICAL CHEMISTRY B

READ 🗹

## Characterization of Photophysical Properties of Photoactivatable Fluorescent Proteins for Super-Resolution Microscopy

Antai Tao, Junhua Yuan, et al.

FEBRUARY 17, 2020

THE JOURNAL OF PHYSICAL CHEMISTRY B

READ 🗹

# Fully Quantum Chemical Treatment of Chromophore-Protein Interactions in Phytochromes

Ronald González and Maria A. Mroginski

NOVEMBER 01, 2019

THE JOURNAL OF PHYSICAL CHEMISTRY B

READ 🗹

# **Unified Model for Photophysical and Electro-Optical Properties of Green Fluorescent Proteins**

Chi-Yun Lin, Steven G. Boxer, et al.

AUGUST 27, 2019

JOURNAL OF THE AMERICAN CHEMICAL SOCIETY

READ 🗹

Get More Suggestions >